A review

Reaction mechanism and strength of slag and fly ash-based alkali-activated materials

Sun, Beibei; Ye, Guang; de Schutter, Geert

DOI
10.1016/j.conbuildmat.2022.126843

Publication date
2022

Document Version
Final published version

Published in
Construction and Building Materials

Citation (APA)
Sun, B., Ye, G., & de Schutter, G. (2022). A review: Reaction mechanism and strength of slag and fly ash-based alkali-activated materials. *Construction and Building Materials*, *326*, Article 126843. https://doi.org/10.1016/j.conbuildmat.2022.126843

Construction and Building Materials 326 (2022) 126843

Contents lists available at ScienceDirect

Construction and Building Materials

journal homepage: www.elsevier.com/locate/conbuildmat

Review

A review: Reaction mechanism and strength of slag and fly ash-based alkali-activated materials

Beibei Sun [a], Guang Ye [b,*], Geert de Schutter [a,*]

[a] Ghent University, Department of Structural Engineering and Building Materials, Magnel-Vandepitte Laboratory, Technologiepark-Zwijnaarde 60, 9052 Ghent, Belgium
[b] Microlab, Section Materials and Environment, Faculty of Civil Engineering and Geosciences, Delft University of Technology, Stevinweg 1, 2628 CN, Delft, The Netherlands

ARTICLE INFO

Keywords:
Slag and fly ash-based alkali-activated materials
Reaction mechanism
Strength control factors

ABSTRACT

Alkali-activated materials (AAM) are known to be environmentally friendly alternatives to cement-based materials because they can potentially reduce greenhouse gas emissions and reutilize industrial by-products/wastes. To study the factors influencing the strength of slag based alkali-activated materials (BFS-AAM), fly ash based alkali-activated materials (FA-AAM), slag, and fly ash-based alkali-activated materials (BFS/FA-AAM), and clarifying their reaction mechanisms, this paper reviews current knowledge about the mechanical properties and the reaction mechanisms of BFS-AAM, FA-AAM, and BFS/FA-AAM. The precursor requirements and the strength control factors are summarized. The control factors for the strength of BFS/FA-AAM are the BFS/binder ratio, the Na_2O/binder ratio, the SiO_2/Na_2O ratio, and the w/binder ratio. Ion concentrations, determined by these control factors, play a decisive role in the development of strength. Generally, the strength is proportional to the BFS/FA ratio. The optimal values of the Na_2O/binder ratio of BFS-AAM and FA-AAM are between 5.5% and 8% and between 7 and 10%, respectively. The optimal values of the SiO_2/Na_2O ratio of BFS-AAM and FA-AAM are between 0.85 and 1.4 and between 0.6 and 1, respectively. Increasing the w/binder ratio will only benefit workability but will affect the strength negatively. A w/binder ratio of around 0.4 may strike a balance between strength and workability.

1. Introduction

It is known that cement production, including $CaCO_3$ calcination and clinker production, is associated with high energy consumption and the emission of a considerable amount of greenhouse gas. The amount of CO_2 released in the production of cement is about one ton for each ton of cement clinker. Almost 8% of the global emission of CO_2 is produced by the cement industry [1]. For the sake of environmental protection, it is vital to search for alternative low CO_2 emission binders for concrete to reduce its carbon footprint. The development of alternative binders utilizing industrial by-products is one of the existing strategies. Despite reduced CO_2 emission, the utilization of industrial by-products also contributes to the ecological cycles and reduces the economic pressure on waste disposal. Currently, only a minor part of this material is utilized (20–30%) on a worldwide basis, while the rest is still disposed of in landfills [1].

Alkali-activated materials (AAM) have attracted attention as a potential replacement for ordinary Portland cement concrete (OPC) [2-4]. Typically, AAM is produced by the alkali activation of silica and alumina-rich materials using alkaline activators. By-products like blast furnace slag (BFS) and fly ash(FA) with rich silica-alumina sources are often used as precursors in AAM. Based on previous research, blast furnace slag-based alkali-activated materials (BFS-AAM) tends to have poor workability, short setting time, and shrinkage, while fly ash-based alkali-activated materials (FA-AAM) are characterized by slow strength development at ambient temperature [5-10]. A good synergy of BFS and FA in AAM could obtain both good mechanical strength and durability [11-16]. BFS/FA-AAM possesses lots of advantages, such as rapid strength gaining, low thermal conductivity, high volume stability, fire resistance, and chemical erosion resistance [17-21].

Even though FA/BFS-AAM has good application prospects, there is still a lack of systematic and comprehensive research on the reaction mechanism and strength development. . Because the strength development mainly relies on the microstructure, it is necessary to conduct an in-depth exploration of the reaction mechanism, and have a better understanding of how each reaction component contributes to strength.

* Corresponding authors.
E-mail addresses: g.ye@tudelft.nl (G. Ye), Geert.DeSchutter@ugent.be (G. de Schutter).

https://doi.org/10.1016/j.conbuildmat.2022.126843
Received 14 July 2021; Received in revised form 4 February 2022; Accepted 9 February 2022
Available online 17 February 2022

Unlike cement, the chemical composition and the particle size of precursors are not uniform. The very different chemical composition of the raw material may result in a very fluctuating strength [22,23]. The main purpose of this study is to understand the factors influencing the strength of BFS/FA-AAM and to clarify their reaction mechanism.

2. Requirement of raw materials

2.1. Blast furnace slag

BFS is a mixture of phase compositions resembling gehlenite ($2CaO{\bullet}Al_2O_3{\bullet}SiO_2$) and akermanite ($2CaO{\bullet}MgO{\bullet}2SiO_2$), with an overcharge-balanced calcium aluminosilicate framework. It has homogenous cementitious and pozzolanic properties [24], and an irregular shape. Though the chemical composition of BFS varies with different ore origins and furnace operation [25], similar SiO_2, CaO content is found in BFS all over the world. The common chemical composition of BFS is shown in Table 1 [26].

The hydration reactivity of BFS could be influenced by its chemical composition [27,28]. An increase of Ca content and a decrease of SiO_2 and Al_2O_3 content in BFS are associated with higher reactivity and a lower polymerization degree. The increase of MgO content could lead to faster reaction and higher strength of AAM because a higher amount of hydrotalcite is formed, which reduces the Al content incorporated in the CASH gel [29,30]. The increase of the content of Al_2O_3 could reduce the strength of AAM at the early stage because of the formation of stratlingite, while the 28d strength shows no significant difference [31]. Except that, minor components have influences that can not be ignored. For example, when the content of S is lower than 2.5%, the reactivity increases with the increase of S content, but when the content of S is higher than 2.5%, it may cause a disorder of the network structure. An adverse effect is shown on the reactivity of BFS when Ti_2O content is more than 4% [32].

Particularly, BFS suitable for alkali activation must meet the requirements of specific chemical composition. A variety of descriptors considering the relationship between the chemical composition of BFS and its reactivity under different application circumstances are proposed [32]. Among them, the most used hydraulic indexes are basicity coefficient(K_b) and quality coefficient(K_q) based on the oxide composition (see Eq.(1), Eq.(2)) [27,28]. Furthermore, Duxson et al. propose an index that includes the importance of the phase separation in glasses to calculate the reactivity of slag [25](see Eq. (3)). The degree of depolymerization (DP) of the glass network is defined as the molar ratio of free Ca to free Si. The higher the value of DP (typically between 1.3 and 1.5), the higher the reactivity of the silicate network.

$$K_b = \frac{CaO + MgO}{SiO_2 + Al_2O_3} \tag{1}$$

$$K_q = \frac{CaO + MgO + Al_2O_3}{SiO_2 + TiO_2} \tag{2}$$

$$DP = \frac{n(CaO) + 2n(MgO) + n(Al_2O_3) - n(SO_3)}{n(SiO_2) - 2n(MgO) - 0.5n(Al_2O_3)} \tag{3}$$

The main reaction components in BFS can be classified into 3 groups [33]: 1) network formers: Si (bond energy with oxygen atom higher than 335 kJ/mol). 2) intermediates: Al and Mg (bond energy between 210 and 335 kJ/mol). 3) network modifiers: Na and Ca (bond energy<210 kJ/mol). It is known that the network formers improve the condensation degree, the network modifiers disorder and depolymerize the network, and intermediates act both as network formers and network modifiers. The combination and content of them eventually determine the glassy phase and crystalline phases in the network, which further influence the reactivity of BFS. Depending on the quenching process, the high polymerized glass phase (Si tetrahedron with more network modifier) and the low polymerized glass phase (Si tetrahedron with more network former) are composed in BFS, as shown in Fig. 1(b) and Fig. 1(c)). Chen et al., [34] found that the best reactivity of BFS is not associated with the lowest polymerization degree of the structure, but with 58% of low polymerized phase. Except that, a small amount of crystalline phase could be precipitated which barely has reactivity (see Fig. 1 (a)). A higher glassy content/crystalline phase ratio is associated with the higher hydraulic reactivity of BFS.

Except for the chemical composition and network structure (glassy phase/crystalline phase ratio) of BFS, the reactivity of BFS could be influenced by its fineness [27,35]. Increasing fineness (high specific surface area) leads to more water requirements and faster settings. Wang et al. revealed that BFS particles larger than 20 um react slowly while particles smaller than 20 um have a chance to completely react after 24 h in AAM [36]. Wan et al. indicated that the more 2–30 um particles, the higher the long-term strength [37]. However, fine BFS particles are not always preferable to coarse BFS particles. Ye et al., [15]. revealed that the increased rate of hydrating layer on coarse particles is higher than that hydrating layer on fine particles. Because coarse particles contain a higher content of CaO but a relatively lower content of MgO, Al_2O_3, and SiO_2 [38]. Shi et al. found that increasing the BFS fineness above 4000 cm^2/g has little effect on 28d strength while remarkably improving the early strength [38,39].

Overall, the hydration reactivity of BFS could be experimentally tested by measuring the strength of the hardened NaOH-activated BFS mortars [40]. Despite that, it could also be evaluated by analyzing the chemical composition, glassy content, and fineness. Wang and Puertas observed that the optimal fineness of BFS that is suitable for AAM is in the range of the Blain value of 4000–5500 cm^2/g considering both properties and economics [35]. The British Standard requires a minimum glass phase content of 90% [41]. To ensure good reactivity, the basicity coefficient should be larger than 1.0, and the quality coefficient should be larger than 1.4 [35,36]. Talling [30] suggested that CaO/SiO_2 ratio should be between 0.5 and 2, while Al_2O_3/SiO_2 ratio should be between 0.1 and 0.6. To avoid the adverse effect, the minor components S and TiO_2 are better to be lower than 2.5% and 4% perspectively as discussed before [40,42]. In conclusion, BFS satisfying the requirements

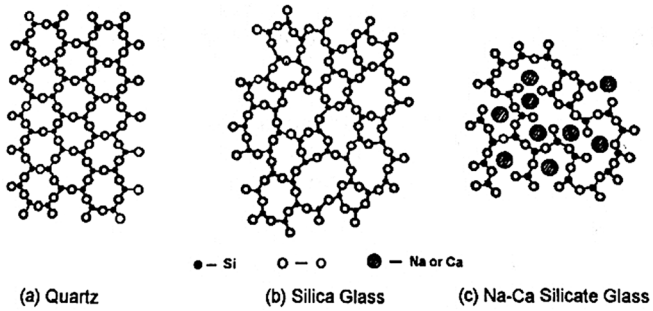

Fig. 1. Two-dimensional representation of the crystalline and glassy structure of BFS [26].

Table 1
Common chemical composition of BFS (wt%) [26].

SiO_2	CaO	Al_2O_3	MgO	Fe_2O_3	S	Cr_2O_3	Na_2O K_2O	MnO_2	P_2O_5	TiO_2
27–40	30–50	5–33	1–2.1	<1	<3	0.003–0.007	1–3	<2	0.02–0.09	<3

in Table 2 is preferable for AAM.

2.2. Fly ash

Fly ash (FA) is mainly composited of SiO_2, Al_2O_3, Fe_2O_3, CaO. The chemical composition varies substantially depending on the impurities in the coal [46]. FA contains different sizes of inhomogeneities spherical particles (parts of them are hollow) [47]. The shape of FA has lots of advantages, such as: reducing the water demand by rolling effect and reducing porosity by maximizing particle packing.

FA could be classified into 2 categories. Generally, the FA with content of $50\% < SiO_2 + Al_2O_3 + Fe_2O_3 < 70\%$ is defined as type C-FA (high calcium FA) [43,48], which is rarely used as a precursor because of too fast setting properties [40]. The FA with the content of $SiO_2 + Al_2O_3 + Fe_2O_3$ greater than 70% is defined as type F-FA (low calcium FA), which has a high content of amorphous alumina-silicate phases [49]. In the 1950 s, Glukhovsky first used type F-FA as a precursor for AAM. Later on, more and more studies have confirmed its application potential in AAM [50-53]. All the FA used below refers to type F-FA. It is worth noting that the chemical content of F-FA is inconsistent between different sources, and specifications for the type F-FA according to EN 450–1 and ASTM C618 are slightly different, as shown in Table 3.

The common chemical composition of FA is shown in Table 4. The high proportion of Si and Al ensured a sufficient glassy phase in FA and leads to a crosslinked aluminosilicate gel. The properties of FA-AAM are mainly controlled by the availability of Al (normally between 21.8% – 34.5%) [54-56]. Without enough reactive Al, the reaction products could be unstable when exposed to moisture, even though the strength development is acceptable. Besides, a high content of loss on ignition (LOI) could lead to high water demand and low strength of FA. Because it increases the content of carbon and reduces the pozzolanic activity. A maximum of 5% and 6% of LOI is specified by EN-450–1 and ASTM C618 (2008), respectively. A maximum of 3% and 5% of SO_3 are allowed in FA, according to EN-450–1 and ASTM C618 (2008), respectively. Despite that, the content of unburnt carbon, the presence of Fe, and sulfate or chloride contamination could also affect the strength [57-60].

The fineness of FA is also a critical factor for the strength development of FA-AAM [62,63]. Fernandez-Jimenez found that the strength of FA-AAM improves dramatically when the mean particle size of FA is lower than 45 μm [43]. Van Jaarsveld [64] reported that the surface charge of FA could influence the initial setting properties. Mechanochemical activation is a promising method to modify the surface chemistry of FA and obtain better reactivity in the early stage of the alkali-activated process [44,65]. Although the effectiveness of mechanochemistry activation has been proved on various silicate materials, a detailed analysis is needed to study its effect on FA.

Overall, the requirement of FA for AAM is presented in Table 5. It includes not only the standard requirements of type F FA as listed in Table 3 but also requirements that ensure the stable performance of FA in AAM based on currently available research.

Table 2
The requirement of BFS for AAM [33,35,43-45].

Physical properties	Chemical properties
Optimal: $4000–5500 cm^2/g$	Basicity coefficient (k_b) $\frac{CaO+MgO}{SiO_2+Al_2O_3} \geq 1$
Glassy phase greater than 90%	Quality coefficient (k_q) $\frac{CaO+MgO+Al_2O_3}{SiO_2+TiO_2} \geq 1.4$
	$0.5 \leq \frac{CaO}{SiO_2} \leq 2$
	$0.1 \leq \frac{Al_2O_3}{SiO_2} \leq 0.6$
	$S \leq 2.5\%$
	$TiO_2 \leq 4\%$

Table 3
Specifications for Type F-FA according to EN 450–1 and ASTM C618 [40,42].

	En 450–1	ASTM C 618
Source	Bituminous coal and anthracite	Bituminous coal and anthracite
Type of binder	Pozzolana	Pozzolana
Requiements	Reactive CaO≤ 10%	CaO, max: no limit
		Amount retained when wet sieve on
	Reactive $SiO_2 \geq$ 25%	–
	LOI< 5%	LOI< 6%
	$SiO_2 + Al_2O_3 + Fe_2O_3 \geq 70\%$	$SiO_2 + Al_2O_3 + Fe_2O_3 \geq 70\%$
	SO_3, max 3%	SO_3, max 5%
	–	Free moisture, max: 3%
	Free lime< 1%	–
	–	45μm: 34%

2.3. Alkaline activators

Alkaline activators of AAM are mainly composed of alkali components (OH^-, SiO_3^{2-}, CO_3^{2-}) and the elements of the first and the second group in the periodic system of elements (Na^+, K^+, Ca^{2+}). Different activators may lead to various mechanical properties of AAM because of different reaction mechanisms. Among all the activators, sodium hydroxide (NaOH) and sodium silicate (Na_2SiO_3) are the most commonly used alkaline activators because of their high efficiency, relatively lower price, and easy production.

NaOH could create a high pH environment for the dissolution of the aluminosilicate in AAM. The viscosity of NaOH increases with the increase of concentration and gently decreases with the rise of temperature [67]. Compared with Na_2SiO_3, it has a relatively higher price due to the large electricity consumption during the production process.

Na_2SiO_3 provides both an alkali environment and soluble Si species in AAM. The SiO_2/Na_2O ratio (also called modulus) of commercial Na_2SiO_3 is usually at 1.6–3.85. With an increasing SiO_2/Na_2O ratio, the reversible hydrolyzation process could be promoted with more H_2SiO_3 generated (see Eq.(4)(5)). When the SiO_2/Na_2O ratio is higher than 2, Na_2SiO_3 may be non-uniform and have poor dissolubility [26]. Oversaturated H_2SiO_3 is prone to crystallization in an array of small species (hydrated sodium metasilicates), which gradually results in the precipitation as a colloidal or gel (not a chemically stable hardened material) [68-70]. The viscosity of sodium silicate is relatively higher than that of sodium hydroxide and decreases with higher temperatures as well [71]. It is reported that the viscosity of Na_2SiO_3 remains the same with the Na_2O concentration lower than 7%, while increased rapidly with the increase of the SiO_2/Na_2O ratio when the Na_2O concentration is higher than 7% [26].

$$SiO_2 + 2OH^- \leftrightarrow SiO_3^{2-} + H_2O \quad (4)$$

$$SiO_3^{2-} + 2H_2O \leftrightarrow H_2SiO_3 + 2OH^- \quad (5)$$

Previous studies have shown that a combination of NaOH and Na_2SiO_3 could stimulate the strength of AAM more effectively [26,72]. The compressive strength of FA-AAM could be maximized when the amount of NaOH added to Na_2SiO_3 reaches a specific value [73]. This is because the addition of NaOH could change the SiO_2/Na_2O ratio of the Na_2SiO_3 solution. As a result, a preferable condition for the alkali reaction is created. The effect of the SiO_2/Na_2O ratio on the strength and the influence mechanism will be discussed later in this paper. Currently, more and more studies use the combination of NaOH and Na_2SiO_3 to explore the best performance of AAM.

Table 4
Common chemical composition of type F-FA (wt%) [61].

SiO_2	Al_2O_3	Fe_2O_3	CaO	SO_3	MgO	K_2O	Na_2O	Reactive Si	Free lime
42.6–59.8	21.8–34.5	6.3–18.1	2.8–7.0	0.19–1.9	1.2–2.6	0.38–6.0	0.15–0.94	0.94	0.74

Table 5
The requirement of FA for AAM [27,42,43,46,47,49,66].

Physical properties	Chemical properties
80%-90% particle≤45 μm glass phase greater than 50%	Reactive $SiO_2 \geq 25\%$ Reactive $\frac{SiO_2}{Al_2O_3} \geq 1.5$ $Fe_2O_3 \leq 10\%$ CaO≤ 10% SO_3≤3% LOI ≤5% Free lime < 1% Free moisture < 3%

3. Reaction mechanism

3.1. Reaction mechanism of BFS-AAM

3.1.1. Reaction process

The reaction process of BFS-AAM takes place mainly in 2 stages: destruction and polycondensation [24]. Based on the research of Glukhovsky and Krivenko [74] during the period 1967–1994, a theoretical model for the reaction mechanism in BFS-AAM is proposed, as shown in Fig. 2.

Isothermal calorimetry studies have been carried out to understand the reaction mechanism of BFS-AAM [72,75-82] activated by NaOH and Na_2SiO_3. The reaction process of NaOH activated BFS-AAM could be divided into 3 stages, as shown in Fig. 3(a)(c). In the first stage, the initial undersaturation degree of reaction ions is large. With the attack of OH^-, the main reaction ions are rapidly released, accompanied by a rapid heat release (the first peak within minutes). During this period, the concentration of reactive ions in the solution gradually increases, and the undersaturation degree decreases again. In the second stage, more and more ions contact each other and progressively form CSH gel on the surface of BFS, which results in a second heat evolution rate peak at around 0.2–24 h [5,31,78,83-85]. During this period, the alkaline cation Na acts as a mere catalyzer to exchange with Ca and form CSH gel (see Eq.(6), Eq.(7), Eq.(8)) [74]. With the advance of the reaction, Al tetrahedrons gradually replace Si tetrahedrons in bridging positions, and Na is taken up into the chain with Al to neutralize the charge imbalance. The uptake of Al turns CSH to CASH and increases the linear chain length. The anion (OH^-, SiO^{2-}) plays an instrumental role in the reaction at this stage. In the third stage, a CASH layer on the surface of BFS continues to grow until the reaction product shell is formed. The OH^- ions cross the shell at a very low speed, and the reaction gradually stops. As a result, a steady period occurs. It is worth noting that the first and second peaks might blend and turn into one peak when the Na_2O/b ratio is high, due to the rapid dissolution and reaction product precipitation [78].

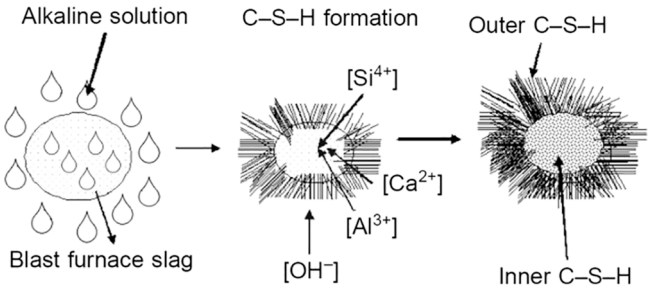

Fig 2. A theoretical model for the reaction mechanism in BFS-AAM [26].

$$= Si - O^- + Na^+ == Si - O - Na \quad (6)$$

$$= Si - O - Na + OH^- == Si - O - Na - OH^- \quad (7)$$

$$= Si - O - Na - OH^- + Ca^{2+} == Si - O - Ca - OH + Na^+ \quad (8)$$

The reaction mechanism of Na_2SiO_3 activated BFS is slightly different from that of BFS activated by NaOH. The reaction process of Na_2SiO_3 activated BFS could be divided into 4 stages, as shown in Fig. 3 (b)(d). Si already exists in the solution. The Si in Na_2SiO_3 is highly soluble and could be taken up in the structure. In the first stage, the undersaturation degree of Si is very low, while that of other reaction ions (Ca, Al) is large. These ions on the surface soon dissolve into the solution and release a large amount of heat (characterized by the first heat evolution rate peak within minutes), while Si remains on the surface. In the second stage, the Si layer on the surface of BFS gradually grows because the dissolution rate of other reaction ions is much faster than that of Si. As long as the thickness of the Si layer exceeds a certain extent, the release of these ions is hindered because they can hardly cross the layer. The reaction slows down, associated with an induction period. In the third stage, the previously released Ca and Al react with soluble Si in the solution and form CASH gel. The formation of CASH gel consumes reaction ions and leads to an increased undersaturation degree. As long as the energy provided by the undersaturation degree overcomes the activation energy barrier, the Si layer dissolves, accelerating more ion release in the solution and the formation of reaction products. At this moment, a second heat evolution peak occurs (at around 5–70 h) [79,84,86-94]. In the fourth stage, the reaction products gradually accumulate not only on the surface of BFS but also in the solution. Reaction product shells on the BFS particles prevent the further dissolution of unreacted BFS. With the slowdown of reaction, a steady period follows. It is worth noting that a peak might occur between the first peak and the second peak at around 0.2–20 h [5,31,85,95,96], when the SiO_2/Na_2O ratio is low, displaying the characteristics of both the BFS-NaOH system and the BFS-Na_2SiO_3 system. This is due to the early precipitation of the primary CSH gel on the surface of BFS particles [97].

3.1.2. Reaction products

As demonstrated in Fig. 4, two layers of reaction products are detected in BFS-AAM [82,98], including a darker inner layer containing denser CSH gel, and a brighter outer layer containing less dense CASH gel. CASH gel (a leaf-like semi-crystalline calcium-sodium aluminosilicate hydrate gel with layered two-dimensional, cross-linked structure) is the predominant reaction product in BFS-AAM. It has a lower Ca/Si ratio (0.8–1.02) than CSH gel generated in OPC and does not have a uniform molecular structure as CSH gel does [99-102]. Besides, a series of secondary products with crystalline phases is also formed, such as hydrotalcite [103], tetra calcium aluminate hydrate [45], katoite, and stratlingite [100]. The structure and composition of CASH gel and the type of secondary product are generally related to the composition of the precursors, the concentration of alkaline activator, and the curing condition [25,54,104-115].

BFS-AAM activated by NaOH has a faster initial reaction rate than that activated by Na_2SiO_3 [78,116]. When NaOH is used as an alkali activator, a higher density of reaction products and semi-crystalline CSH gel could be detected on the first day [78]. The coarse porosity decreases very slowly after the first day, resulting in many detectable pores at 28 days (see Fig. 5(a)). The chemical composition of the inner and outer

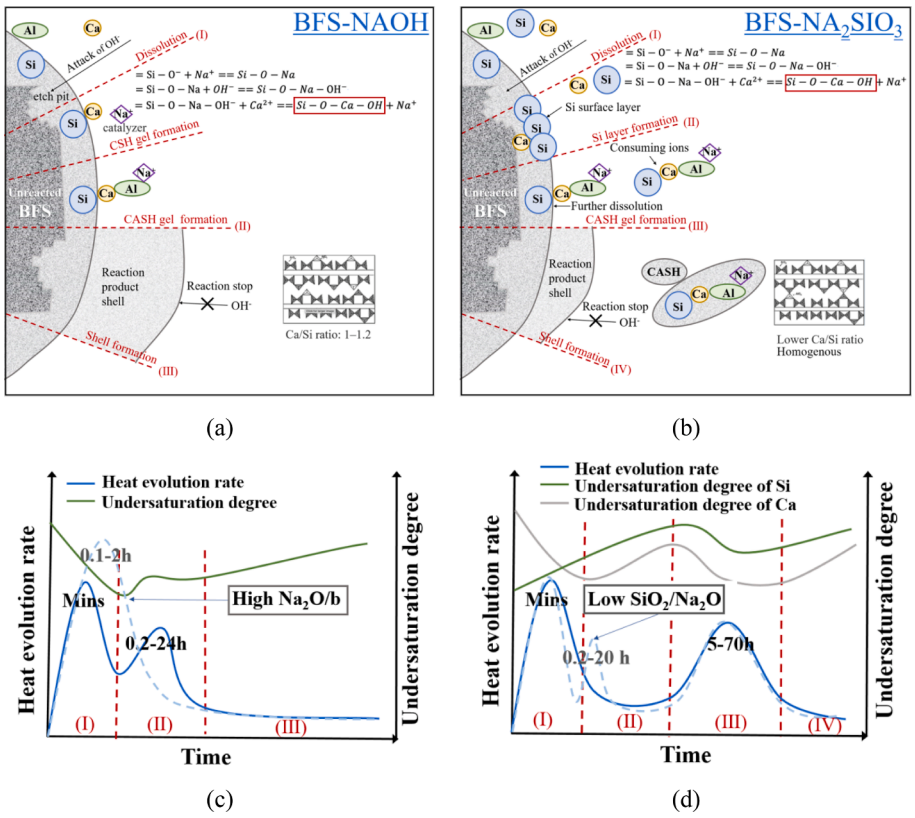

Fig. 3. Reaction process of BFS-AAM: (a) reaction stages of BFS-NaOH system; (b) reaction stages of BFS-Na_2SiO_3 system; (c) hydration heat and undersaturation degree evolution in BFS-NaOH system; (d) hydration heat and undersaturation degree evolution in BFS-Na_2SiO_3 system.

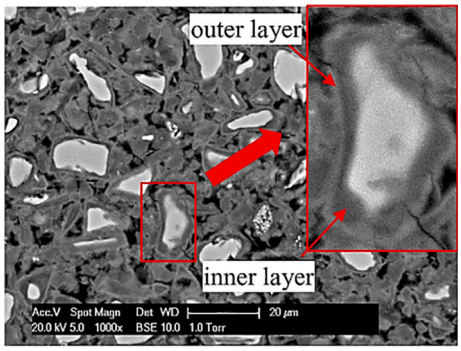

Fig. 4. Microstructure of NaOH activated BFS-AAM at 28 days [82].

reaction products of BFS-AAM is shown in Fig. 6(a). Although the Al/Si ratio, and Ca/Si ratio of the inner and outer layers are similar, more Na has been observed in the outer layer because the coarse and porous structure of the outer layer enables more Na_2O filling in the pores. The outer layer is an accumulation of reaction products on the surface of BFS initially occupied by the solution, which could be observed after around 3 h depending on the properties of BFS and alkali activator [102]. While the inner layer occurs probably after 6 h and CSH gel could be still increasing after 180 days [78,116]. XRD is not suggested in tracking and identifying the binding compounds produced in AAM, due to the presence of large amorphous CASH gel (around 95 %) and undetectable crystalline CSH in the solution with a pH higher than 14 [112,117]. Nevertheless, NMR has proved to be an effective method because the chemical shift (PPM) can reflect the coordination situation of polymer core Al ions and Si ions. The ^{29}Si and ^{27}Al MAS NMR spectra study of NaOH activated BFS-AAM is presented in Fig. 7(a) and Table 6. High

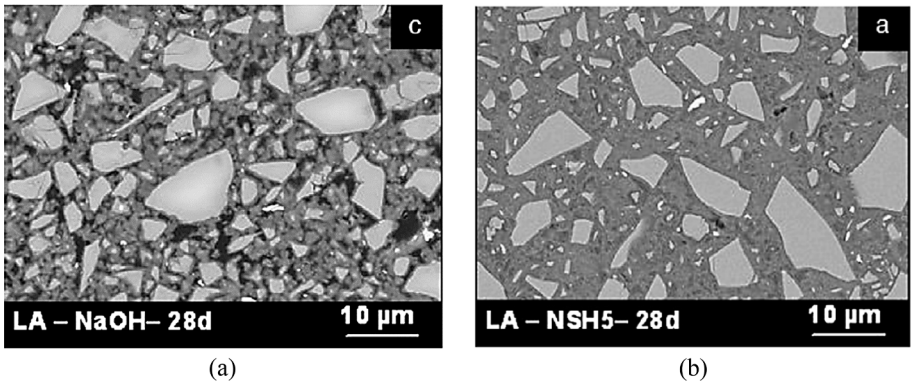

Fig. 5. (a) SEM image of NaOH activated BFS-AAM (b) SEM image of Na_2SiO_3 activated BFS-AAM (LA refers to low Al slag, NSH5 refers to Na_2SiO_3) [116].

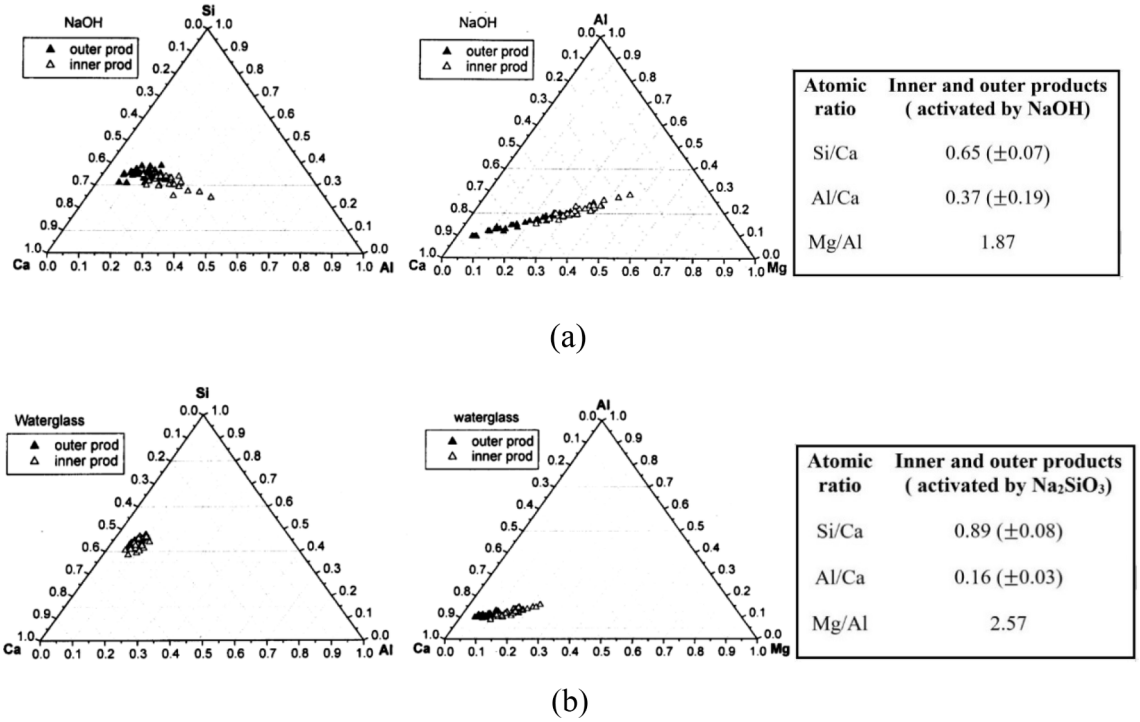

Atomic ratio	Inner and outer products (activated by NaOH)
Si/Ca	0.65 (±0.07)
Al/Ca	0.37 (±0.19)
Mg/Al	1.87

Atomic ratio	Inner and outer products (activated by Na_2SiO_3)
Si/Ca	0.89 (±0.08)
Al/Ca	0.16 (±0.03)
Mg/Al	2.57

Fig. 6. Chemical composition of the reaction products of BFS-AAM: (a) activated by NaOH; (b)activated by Na_2SiO_3 [116].

content of Q^2 units and nearly no Q^3 units is observed. This points to long linear chains of CASH gel [114]. Richardson et al. proposed a series of equations to calculate the mean Si chain length and the Si/Al ratio in CASH gel by NMR data [100,118].

Although the reaction products in Na_2SiO_3 activated BFS-AAM develop slower compared with NaOH activated BFS-AAM, they could precipitate uniformly throughout the interstitial space between BFS particles. When Na_2SiO_3 is used as an alkali activator, a higher coarse porosity is detected at an early age, and the bonds between reaction products keep developing. The pore space is gradually filled after 7 days. A large amount of highly condensed uniformly amorphous phase is formed, and a homogenous microstructure could be detected at 28d (see Fig. 5(b)). The crystallinity remains very low after a year of reaction. Besides, the thickness of the reaction product layer of AAM activated by Na_2SiO_3 is much higher than that activated by NaOH [116]. The CASH gel in the Na_2SiO_3 activated system incorporates more water than that in a NaOH activated system [30,99]. The Ca/Si ratio of the inner layer is higher than that of the outer layer. Because the inner layer is Si gel

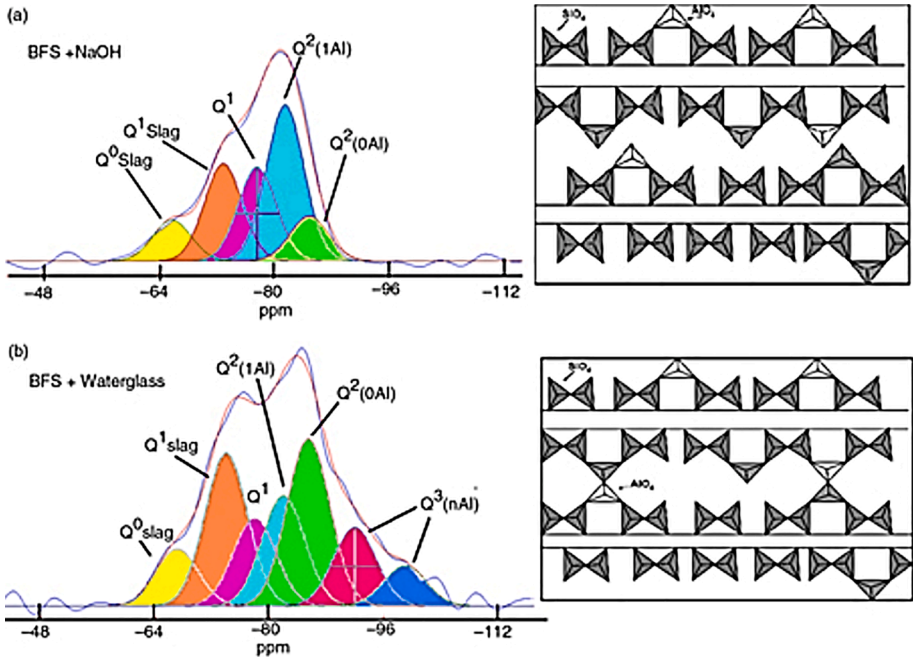

Fig. 7. Structural model for Al-containing C-S-H gel: (a) linear chains activated by NaOH; (b) linear chains with occasional cross-linking, forming planes, activated by Na_2SiO_3 [113].

Table 6
Results from 29Si and 27Al MAS NMR spectra of BFS-AAM (7d) [114].

Sample		Q^0 (BFS)	Q^0/Q^1 (BFS)	Q^1 (chain end)	Q^2 (1 Al)	Q^2 (0 Al)	Q^3 (1 Al)	Q^3 (0 Al)	Al_T	Al_P	Al_O
BFS	Pos. (ppm)	−59.1	−74.0						60.81	32.62	10.02
	Width	7.62	13.38						32.66	23.85	23.39
	Intergral(%)	6.2	93.8						81.57	12.22	6.22
NaOH	Pos. (ppm)	−65.9	−73.0	−77.69	−81.60	−85.00			60.87	30.43	8.82
	Width	6.26	6.26	6.26	6.26	6.26			22.89	18.94	10.83
	Intergral(%)	9.43	22.53	36.05	36.05	10.26			77.65	6.48	15.87
Na2SiO3	Pos. (ppm)	−67. 12	−74	−78	−82	−85.5	−92	−97.00	61.79	32.89	8.25
	Width	7.05	7.05	7.05	7.05	7.05	7.05	7.05	21.727	22.05	12.22
	Intergral(%)	9.12	22.05	12.61	15.86	24.07	11.37	5.80	75.80	7.60	16.60

modified with Ca and Al, while the outer layer is a deposit of Si at the early stage (see Fig. 6(b)) [116,119]. According to the NMR spectra studies, a substantial number of Q^4(1Al) (103–115 ppm) and Q^3(nAl) (95–100 ppm) units, along with Q^1(0Al) (74–78 ppm) and Q^2(0Al) (83–88 ppm) units could be identified. The polymerization degree increase with more Al incorporated in CASH gel over time [120], which eventually leads to a cross-linked and highly condensed structure (see Fig. 7(b) and Table 6).

3.2. Reaction mechanism of FA-AAM

3.2.1. Reaction process

Glukhovsky developed the initial reaction mechanism of alkali-activated aluminosilicate materials in the 1950–1970 s [74]. Conceptually, the reaction mechanism of FA-AAM is divided into 3 stages, which include destruction-coagulation, coagulation-condensation, condensation-crystallization. Palomo [113] divides the reaction mechanism of FA-AAM into 2 stages: nucleation and growth based on zeolite synthesis. John Provis [54,115,121,122] proposed the first detailed mechanistic model for FA-AAM, as shown in Fig. 8. Subsequently, a series of specific mathematic models have been developed [123,124].

In FA-AAM, the critical network formers are Al and Si. The Ca and Mg act as network modifiers, providing the charge balance required by tetrahedral Al as well as any depolymerized framework sites. The reaction chemical equations for FA-AAM are listed as below (see Eq.(9), Eq.(10), Eq.(11)) [74]:

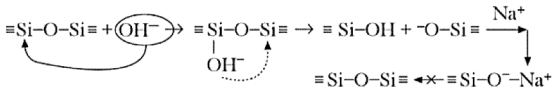

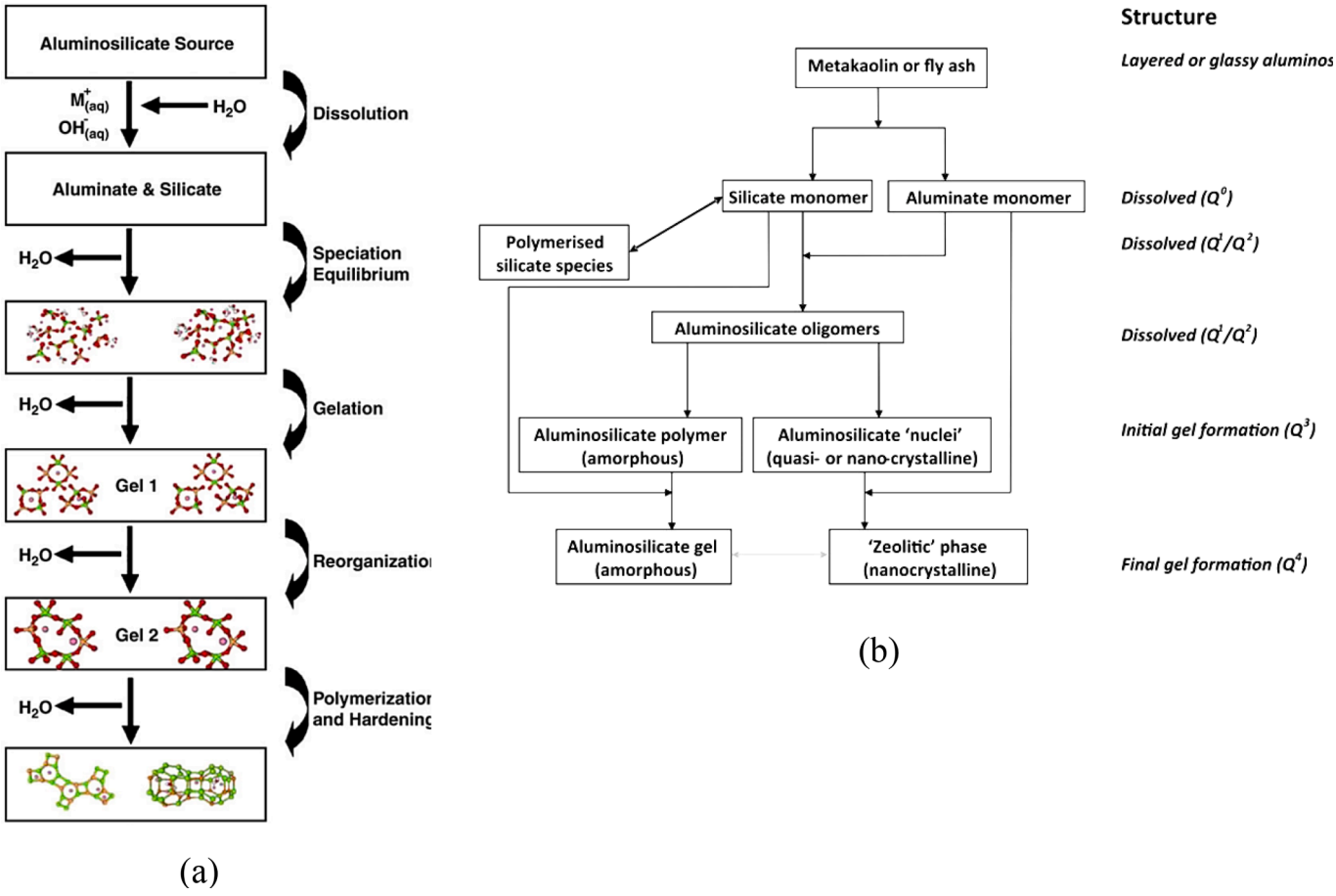

Fig. 8. Reaction sequence of polymerization [54,115].

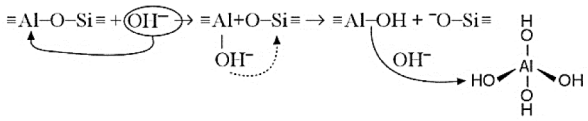

of Si-O-Na prohibits the reversion of Si-O-Si. Duxson found that when the NASH gel has a Si/Al ratio under 1.4, Na present in the pore solution mainly neutralizes the negative charge of $Al(OH)_4^-$ groups [131]. The first heat evolution rate peak (within minutes) accompanies the destruction process. The second stage is associated with an induction period. The released Al monomers are continually absorbed on the surface of FA because of the passivation effect [132]. Accordingly, the equilibrium solubility of the FA particles concerning Si is dramatically

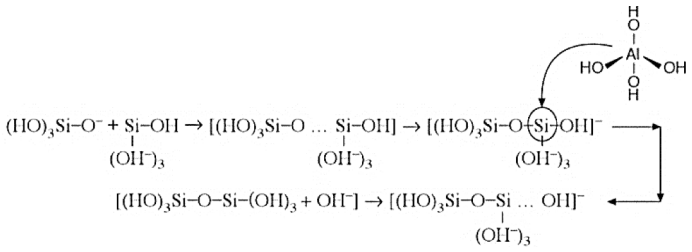

Based on the isothermal calorimetry study [16,80-82,125-127], the reaction process of NaOH activated FA could be divided into 4 stages, as shown in Fig. 9(a)(c). In the first stage, the OH^- redistribute the electronic density around the Si, breaking the Si-O-Si bonds and Si-O-Al bonds into Si-OH, $Al(OH)_4^-$, and Si-O-. The network breakdown rate during the non-uniformed dissolution is associated with the chemical composition of the precursors [128]. Previous research has shown that Si-O-Si bonds are stronger than Si-O-Al bonds, and the bonds between network forming species and network modifying species are the weakest [103,127,129,130]. Na in the solution acts as a catalyzer at this stage. It neutralizes the negative charge of Si-O- to form Si-O-Na. The formation reduced. In the third stage, more and more reaction ions are dissolved into the solution. When the amount of reaction ions exceeds a certain level, they contact each other and begin to polycondensate on the surface of FA [133]. This process gradually consumes Al, reducing the thickness of the Al layer, and promoting the further release of reaction ions. A large amount of heat is released by the polycondensation process, resulting in the second peak at around 1–24 h [110,134-136]. Within this period, OH^- acts as a catalyzer, while Na acts as a structural component. The network modifiers are also induced into the structure to neutralize the charge imbalance of Al. When the amount of network modifying cations exceeds the requirement of neutralization, they tend to associate with Si, because the tetrahedral Si sites have a higher

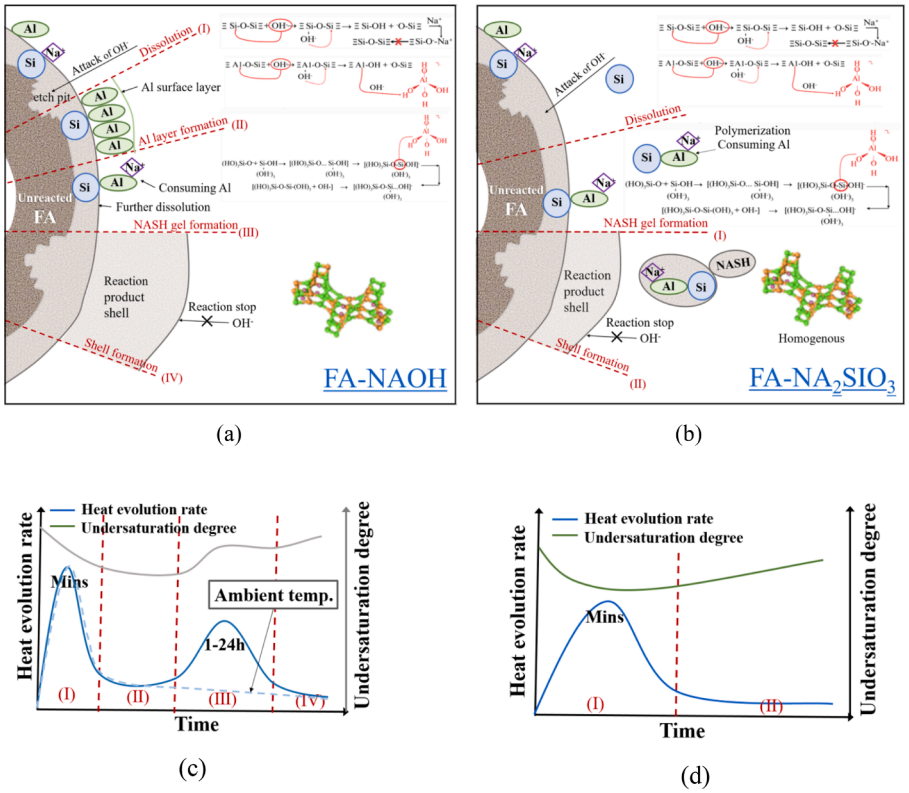

Fig. 9. Reaction process of FA-AAM: (a) reaction stages of FA-NaOH system; (b) reaction stages of FA-Na_2SiO_3 system; (c) hydration heat and undersaturation degree evolution in FA-NaOH system; (d) hydration heat and undersaturation degree evolution in FA-Na_2SiO_3 system.

tendency to host nonbridging oxygen atoms [137]. In the fourth stage, the reaction products accumulate and form shells on the surface of FA [133]. The shell prevents the further diffusion of OH^- on the unreacted FA, and the reaction will stop. This is characterized by a steady period. It is worth noting that the second peak might not exit when FA is activated at ambient temperature (under 35 °C), due to the low reaction rate [16,81,125,138-140].

The reaction rate of Na_2SiO_3 activated FA-AAM is much faster than that of NaOH activated FA-AAM, as shown in Fig. 9(b)(d). The soluble Si in the solution could capture more released Al monomers and form polymers in the solution. As long as these polymers grow and create nuclei sites, the accumulation of reaction ions on nuclei sites is accelerated, building a denser structure in the solution. Despite that no Al layer is formed on the surface of FA, the contribution of nuclei sites simultaneously promotes both the destruction process and the polymerization process. This leads to a broad heat evolution peak in the first stage. Gradually, reaction product shells are formed on the surface of FA and prevent further reaction. A steady period occurs.

3.2.2. Reaction products

Fernendez-Jimenez investigated the microstructure of FA-AAM by SEM. The unreacted particles, particles under attack (with cavities), and reaction products are detected, as shown in Fig. 10 [43,133,141]. The process of reaction begins with a chemical attack of OH^- on the surface of FA, resulting in small cavities in the particles. Following this, the inside of the FA particle is exposed to the alkali-activated solution. More and more reaction products precipitate and cover both inside and outside the FA particle wall.

The main reaction product of FA-AAM is an amorphous aluminosilicate hydrate gel (Na_n-(SiO_2)-(AlO_2)n·wH_2O). Where "n" is the degree of polymerization. The Si and Al tetrahedral incorporate randomly in the 3-dimensional skeleton [17,43,142]. A plan view projection of the structure of the NASH gel is shown in Fig. 11 [143]. The structure is highly determined by the Si/Al ratio. The Si/Al ratio increases with time, which eventually increases the degree of polymerization. It is worth noting that the distribution of Al is not entirely random. According to the 'Loewenstein rule' [144], the Al-O bond could connect with Si or other small ions with electrovalency of not<4. But only Al with a coordination number larger than 4 could be connected with Al and form Al-O-Al bonds, which are strongly disfavoured in tetrahedral structures. Therefore, the minimum Si/Al ratio is 1. Studies have proven that the Q^4(nAl) (n = 0,1,2,3,4) units are predominant in NASH gel. The amorphous NASH gel has a similar chemical composition but no extensive crystalline structure as natural zeolitic. The secondary reaction products of FA-AAM are crystalline zeolitic phases, including hydroxy sodalite, zeolite P, Na-chabazite, zeolite Y, and faujasite [17,47,54,110,142].

3.3. Reaction mechanism of BFS/FA-AAM

3.3.1. Reaction process

Considering all aspects, the combination of raw materials can provide AAM with more excellent comprehensive performance. The advantages of using a combination of BFS and FA as a precursor and using a combination of NaOH and Na_2SiO_3 as an activator have been elaborated in section 2. The above studies on the reaction mechanism of BFS-AAM and FA-AAM activated by NaOH and Na_2SiO_3 respectively provide a foundation for the understanding of this more complex system. The reaction mechanism of BFS and FA alkali-activated by NaOH and Na_2SiO_3 could be divided into 5 stages based on isothermal calorimetry study [82,134,145-148], as shown in Fig. 12 and Table 7. In literature, the optimal value and occurrence time of the peak of heat evolution rate can vary a lot between different systems, and different stages may emerge, appearing as another type of curve. This is due to the effect of control factors on the reaction process, which will be discussed later.

In the initial stage, the undersaturation degree of modifying elements is very large. As a result, a large amount of elements is released. It is known that higher alkaline earth cation gives rise to the degree of framework disorder, nonbridging oxygen atoms content as well as the

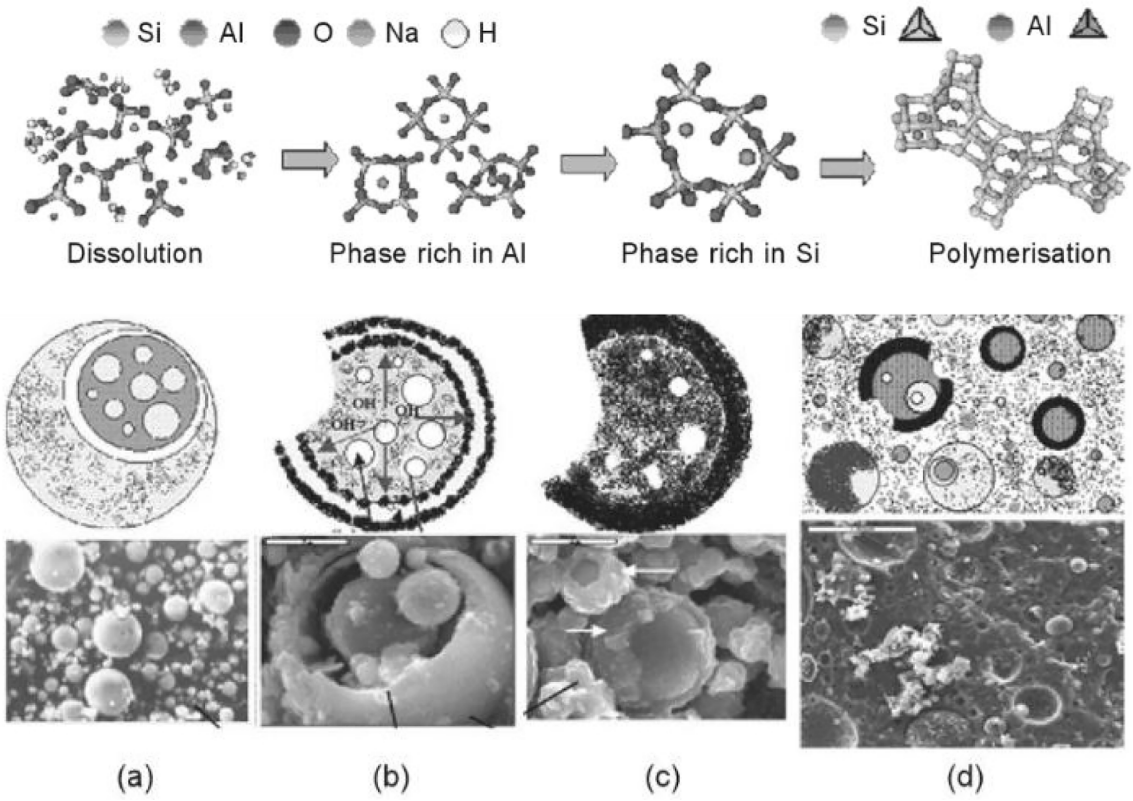

Fig. 10. Microstructure of FA-AAM and formation of NASH gel over time [133,141].

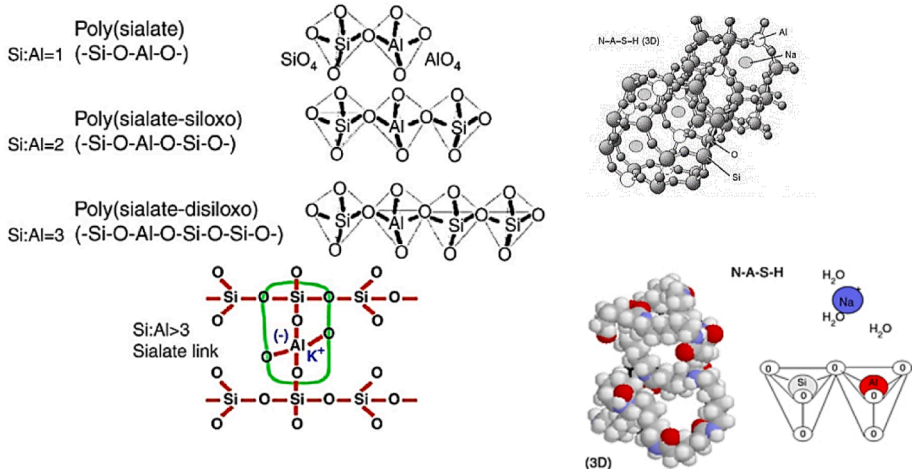

Fig. 11. Structure model for NASH gel [113,143].

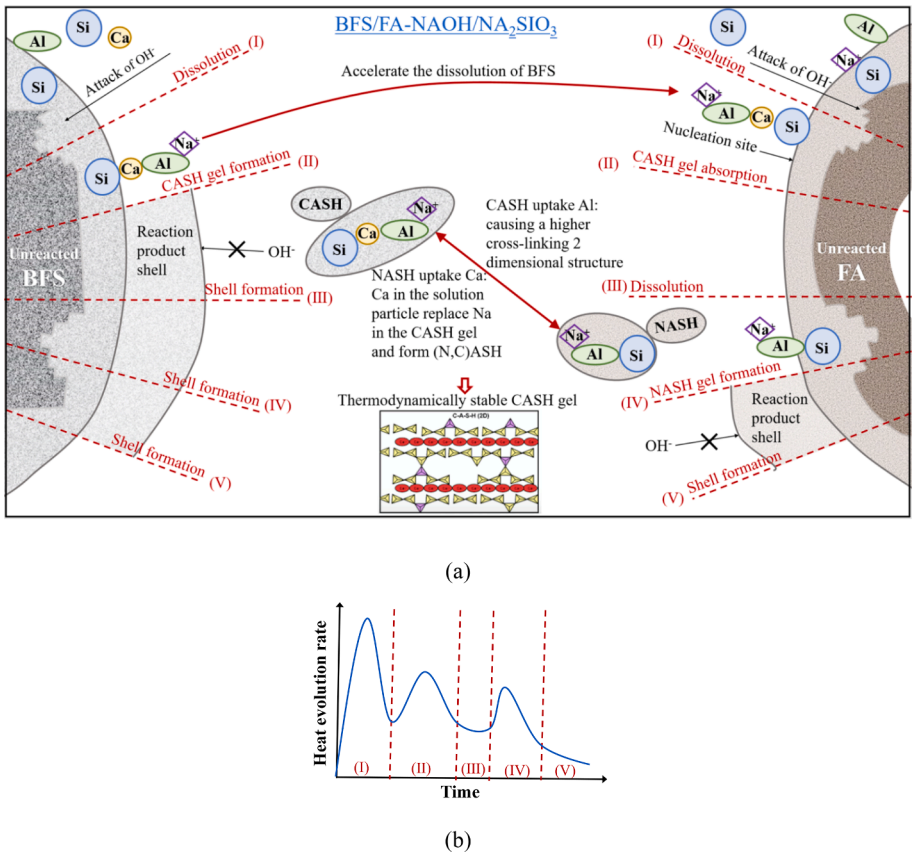

Fig. 12. (a) Reaction process of BFS/FA-AAM; (b) A theoretical heat evolution rate curve of BFS/FA-AAM.

Table 7
Characteristics of the reaction process of BFS/FA-AAM.

Heat evolution characteristics	Reaction process
First peak	Dissolution
Second peak	Formation of CASH gel
Induction period	Formation of reaction product shells on the surface of BFS particles
Third peak	Polymerization of NASH gel
Steady period	Formation of reaction product shells

formation of little content of weak and reactive Al-O-Al bonds [137,149]. BFS contains a more substantial amount of Ca and Mg and less Al than FA. Because the Ca-O-Si bonds and Mg-O-Si bonds, Al-O-Al bonds are much weaker than the Al-O-Si bonds, the dissolution rate of BFS is faster than that of FA. The first heat evolution rate is mainly caused by the dissolution of BFS.

In the second stage, the formation of CASH gel is characterized by the second heat evolution peak. The initial undersaturation degree of Si is low while that of other reaction ions is large. A Si layer may accumulate on the surface of BFS particles because the dissolution rates of other reaction ions are faster than that of Si. And the Si layer may prohibit other reaction ions from crossing through. However, the passive effect is

eliminated to some extent because of the existence of FA particles. During the dissolution, the FA particles could act as nuclear sites, capturing the reaction ions released by BFS [128]. Therefore, CASH gel is not only formed on the surface of BFS but also on the surface of FA. The formation of CASH gel consumes ions, leading to a rapid increase of the undersaturation degree and promoting the release of reaction ions.

In the third stage, a reduction period occurs. During this period, the reaction products on the surface of BFS accumulate and form shells (outer layer). The shell gradually hinders the further reaction of unreacted BFS. The dissolution of the low polymerized phase (Ca-rich phrase) leaves over a spongy and porous surface of BFS. The surface area of the high polymerized phrase (Si-rich phase) is greatly increased, ensuring the increasing strength of the later stage, and an inner reaction layer is gradually formed. However, the reaction rate of the inner layer is slow because of the prevention of the outer layer. In the meantime, the FA particle is still mainly under the destruction period, because of its relatively lower reactivity at the ambient curing temperature.

In the fourth stage, sufficiently high content of reaction ions and nucleation sites in the solution around FA particles accelerates the polycondensation of a large amount of NASH gel [150]. The generated NASH and CASH gel have different structures than those in a single precursor system because they do not develop separately but interact with each other in the further reaction process [26]. An exchange of Al and Ca ions proceeds in the restructuration of CASH and NASH gel.

In the fifth stage, the reaction produces a shell that gradually forms on the surface of the FA particle, and the dissolution is therefore ceased. In the meantime, a thermodynamically stable CASH gel will be created if time is long enough [113,151,152]. This is characterized by a steady period.

Within the formation process of CASH and NASH gel, the concentration of different ions is changing with time and results in the various structures of reaction products at different stages. It is of great importance to understand how these ions affect the structure of the reaction products. The roles of the main reaction ions(Si, Ca, Al, Na, OH^-) acting in the construction of CASH and NASH gels are summarised as follows:

Higher content of Si could increase the polymerization and mechanical properties of both CASH and NASH gels because Si-O-Si bonds are stronger than other bonds. More soluble Si added into the reaction system could not only increases the formation of reaction products but also create a more homogenous structure because of the even distribution of reaction products. Furthermore, when SiO_4 is excessive, polymerized SiO_4 could be precipitated, leading to a denser microstructure. Despite the positive effect of SiO_2, It is reported that too much SiO_4 could hinder the precipitation of zeolite crystals. And lead to volume instability because of the formation of ettringite.

In CASH gel, the higher content of Ca increases the disorder of the structure, including the formation of a small concentration of Al-O-Al when Al content and nonbridging oxygen atoms are high enough. But the amount of Ca being up taken into CSH gel is constant from the beginning of hydration [153]. The rest of Ca reacts with Al and forms the AFm phase. In NASH gel, the Ca in the solution partially replace Na in the NASH gel and form (N, C)ASH gel, because they have a similar ionic radius and electronegative potential [154]. The increase of Ca content is associated with lower porosity and higher strength [155-158].

A series of hydrolysis reactions would happen when Al is in contact with water (see Eq.(12–17)). Al trivalent ions are initially hexatolyic octahedrons in water [159]. When the pH is higher than 8, Al become tetragonal and exists as mainly $Al(OH)_4^-$. But if the network modifying ions is not enough to fully coordinate with Al and keep the charge balance, the $Al(OH)_4^-$ could be primarily reduced, and becomes hexatolyic octahedron with 6 coordination again [25]. As a result, more Al-O-Al would exist in the structure, causing framework disorder. The Al increases the linear chain length as well as the possible existence of sporadic inter-chains, leading to a higher cross-linking structure. The amount of incorporated Al could be higher with higher temperature, humidity, and concentration of alkaline activators. The release rate of Al from FA is considerably slow and highly depends on the type and concentration of alkaline activators [47,57,157].

$$\mathrm{Al}(H_2O)_6^{3+} + H_2O \leftrightarrow Al(OH)(H_2O)_5^{2+} + H_3O^+ \quad (12)$$

$$\mathrm{Al(OH)}(H_2O)_5^{2+} + H_2O \leftrightarrow Al(OH)_2(H_2O)_4^{+} + H_3O^+ \quad (13)$$

$$\mathrm{Al(OH)_2}(H_2O)_4^{+} + H_2O \leftrightarrow Al(OH)_3(H_2O)_3^{0} + H_3O^+ \quad (14)$$

$$Al^{3+} + 4H_2O \leftrightarrow Al(OH)_4^- + 4H^+ \quad (15)$$

$$2\mathrm{Al} + 6H_2O \leftrightarrow 2Al(OH)_3\downarrow + 3H_2 \quad (16)$$

$$Al(OH)_3 + NaOH \leftrightarrow Na[Al(OH)_4] \quad (17)$$

In CASH gel, Na acts as a mere catalyzer to form CSH gel at the early stage. Later on, a part of Na is taken up into the chain with tetrahedral Al to neutralize the charge imbalance caused by AlO_4^-, while the others stay in the solution to neutralize the charge on the $Al(OH)_4^-$ groups [131]. In NASH gel, Na neutralizes the negative charge of Si-O- and form Si-O-Na, preventing the reversion of Si-O-Si [133]. It is directly uptaken into the structure with Al. In both reaction products, Na is present in non-framework sites and associated with oxygen atoms, instead of being located directly next to Al atoms. Nonetheless, excess Na may react with CO_2 in the atmosphere and form white carbonate or bicarbonate crystals on the surface of the materials (see Eq.(18), Eq.(19)), thus causing efflorescence [160,161]. Sealed curing and adding an Al-rich secondary binder are effective ways to control efflorescence.

$$2\mathrm{NaOH} + CO_2 \leftrightarrow Na_2CO_3 + H_2O \quad (18)$$

$$\mathrm{Na_2CO_3} + H_2O + CO_2 \leftrightarrow 2NaHCO_3 \quad (19)$$

The main effect of OH^- in the solution is to break and hydrolyze bonds into Si-OH, Al-OH, etc. Under the attack of OH^- in the solution, different bonds of precursors have different breaking energies which leads to different dissolution rates. the bonds between network forming

Table 8
Reaction products of BFS/FA-AAM [54,112,151,153,154,159,160,162,163].

Reaction products	Chemical composition	Physical property
CASH	Na_n-$(CaO)_m$-$(Al_2O_3)_n$-$(SiO)_2$·wH_2O	A leaf-like semi-crystalline gel Layed 2-dimensional, cross-linked structure
Hydrotalcite	$Mg_6Al_2CO_3(OH)_{16}·4H_2O$	Layers of brucite ($Mg(OH)_2$) with interstitial water molecules and CO_3^{2-} ions. Hydrotalcite crystals are scattered throughout the CASH gel
Tetracalcium Aluminate hydrate	$Ca_3Al_2O_6$	Tetracalcium leads to the phenomenon of "flash set" (instantaneous set), and a large amount of heat is generated.
AFm phase	$3CaO·Al_2O_3·CaSO_4·12H_2O$	AFm phase contribute little to strength development
Calcite	$CaCO_3$	Mohs hardness of 3, a specific gravity of 2.71
NASH	Na_n-(AlO_2)n-(SiO_2)•wH_2O	Amorphous gel, 3-dimensional skeleton, lower space-filling capacity than CASH gel
Zeolite (Hydroxysodalite, Zeolite P, Na-chabazite, Zeolite Y, Faujasite)	Ca_nNa_m [$(AlO_2)_x$ $(SiO_2)_y$] ·n(H_2O)	Cavities are formed in the crystal, and a lot of water molecules are wrapped in it, which forms a porosity structure

C = CaO, S = SiO_2, A = Al_2O_3, N = Na_2O, H = H_2O

species and network modifying species are easiest to break, and Si-O-Al bonds are weaker than Si-O-Si bonds. Besides, when the concentration of OH^- is high, the dissolution of $Ca(OH)_2$ could be decreased, and the dissolution of CSH could be increased.

3.3.2. Reaction products

The reaction products of BFS/FA-AAM are shown in Table 8. Both micro and nanostructure research has shown that a complex mix of amorphous CASH and NASH gels are formed at an early age (28 days) [54,112]. As the main reaction products, the percentage and structure of them mainly depend on both the BFS/binder ratio (binder refers to the mass of all precursors) and the chemical composition of alkaline activators. They directly determine the properties of BFS/FA-AAM.

Specifically, the structure of reaction products dynamically changes with the concentration of Ca/(Si + Al) ratio, Al/Si ratio, OH^- in the pore solution. The results from NMR analysis show that lower Ca/(Si + Al) ratio and higher Al/Si ratio are associated with higher polymerization of reaction products because more NASH gel is formed. Reaction products with more Q^4 and Q^3 units were detected when the BFS/binder ratio is 10%. While reaction products with Q^1 and Q^2 units, but without Q^3 and Q^4 units were observed when the BFS/binder ratio is 30–50%. Moreover, when the OH^- content is high (pH higher than 12), CASH gel is preferentially formed instead of NASH gel.

The ion concentration not only determines the amount of different gels in the initial stage but also makes the gel structure change slowly in the long-term reaction. On the one hand, the Ca in the solution gradually distort the Si-O-Al bonds and create new Si-O-Ca bonds, because of the polarizing effect. As a result, higher Ca content and lower Al content are increasingly found in the structure of NASH gel, which turns NASH gel into (N, C)ASH gel with a more depolymerized structure. On the other hand, the released Al form NASH gel and is then uptaken by CASH in the bridge position to build a 2-dimensional structure with a higher cross-linking chain. Ultimately, the formation of a single 2-dimensional CASH gel (most thermodynamically stable) is the final trend [151].

4. Control factors and mechanisms

The mechanical properties of BFS/FA-AAM mainly depend on the structure and chemical composition of the reaction products, while the reaction products at different ages are closely related to the ions concentration and the reaction in the system as discussed above. Lots of researchers have studied the effect of factors on the strength of BFS/FA-AAM. However, there is no uniform definition of control factors since the composition and concentration of raw materials vary a lot, especially for the activators. For example, a large number of studies focus on the effect of alkali activators/ precursor ratio, $NaOH/Na_2SiO_3$ ratio, which results in a nonrepeatable mix proportion because the modulus of Na_2SiO_3 varies and the alkali concentration is confusing. It is worth noting that any change of the Na_2SiO_3 modulus and $NaOH/Na_2SiO_3$ ratio is indeed changing the initial reaction ion contents thus influencing the reaction process. To avoid misunderstanding, it is important to use the main control factors to directly represent the effect of other various factors.

Four factors have proved to be the control factors of reaction and strength of BFS/FA-AAM: BFS/b ratio, Na_2O/b ratio, SiO_2/Na_2O ratio, and w/b ratio [10]. Among them, w refers to water, b refers to the binder, and all ratios refer to mass ratios. BFS/b ratio represents the reaction capacity of precursors because it can roughly reflect the proportion of Ca and Al in the systems. Na_2O/b ratio represents the intensity of the alkali-activated reaction because it reflects the OH^- content in the system. SiO_2/Na_2O ratio represents the compactness of the structure since it reflects the Si content in the solution. w/b ratio represents the original pores that are introduced in the system. The effects of these control factors on the reaction process and mechanical properties of BFS/FA-AAM are discussed below.

4.1. BFS/b ratio

As shown in Fig. 13(a) [9,146,148,164-171], there is a strong linear relationship between the BFS/binder ratio and 28 d compressive strength. The results indicate that the higher the content of BFS, the higher the strength. Because the increase of BFS content is associated with an increase of Ca and a decrease of Al in the reaction system. The dissolution rate could be faster at the beginning since Ca-O-Si bonds are weaker than Al-O-Si bonds. As the process advances, because the number of nuclei sites (FA) is reduced, the Si layer may form on the surface of BFS earlier, which hinders the further dissolution of reaction ions. Eventually, more CASH gel and less NASH gel could be formed, which would lead to a lower polymerization degree, a higher cross-linking chain reaction product, and a denser microstructure [172-175].

It seems that FA only slightly contributes to the strength at 28 d. This is probably because of the low reactivity of FA. As discussed in the reaction mechanism, the formation of NASH gel is later than the formation of CASH gel. At 28 days, FA has a lower hydration degree than that of BFS. The hollow spherical particle of FA creates lots of pores in the materials since the time is insufficient for the precipitate of reaction products to fill the hollow space [152]. The pores created by FA eventually cause stress concentrations in the materials thus resulting in a decrease in strength. However, researchers have found that the strength of BFS/FA-AAM keeps developing for 90 days for the sake of FA. As

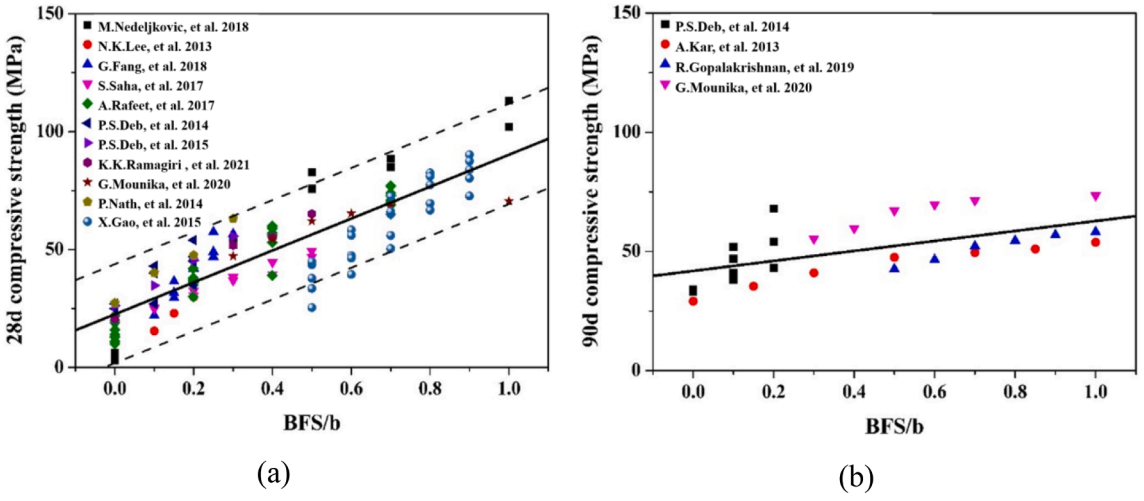

Fig. 13. Effect of BFS/binder ratio on the compressive strength of BFS/FA-AAM [9,146,148,164-171].

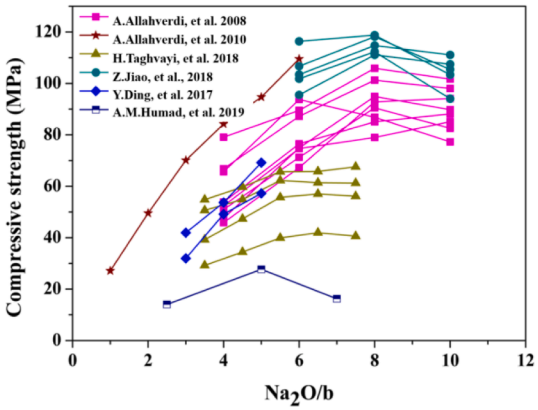

Fig. 14. Effect of Na_2O/b ratio on the compressive strength of BFS/FA-AAM [178-183,199].

shown in Fig. 13 (b) [167,170,176,177]. The slope of the BFS/b ratio and strength at 90 days becomes smaller compared to that of the strength at 28 days. It indicates that more NASH gel is formed later and gradually fills the pores. FA plays a role for a longer reaction period and keeps contributing to the strength till 90 days. Therefore, 90 days of curing is suggested for BFS/FA-AAM.

4.2. Na_2O/b ratio

The effect of the Na_2O/b ratio on the compressive strength of BFS/FA-AAM is shown in Fig. 14 [178-183]. The data includes both paste and concrete samples. There is an optimal value of the Na_2O/b ratio to obtain the highest compressive strength of BFS/FA-AAM. The strength first increases with the Na_2O/b ratio. Because higher content of OH^- increases the dissolution of BFS and FA. Accordingly, the higher content of released monomers has a higher tendency to be connected. Moreover, a higher amount of free ions and a high amount of catalyzer (Na) also improve the formation rate of CSH gel.

However, when the Na_2O/b ratio exceeds a specific value, the strength may begin to decrease. When the concentration of OH^- is high, the dissolution of $Ca(OH)_2$ is reduced, and a thin layer of $Ca(OH)_2$ is formed on the surface of BFS particles. So Ca is less capable of reacting with Al and Si and forming the CASH gel. What is more, excess OH^- causes Al-Si gel precipitation at the very early stage on the surface of the FA particles, so the subsequent polymerization is hindered, and the strength is therefore decreased. Excess Na may also cause efflorescence and reduce the strength to some extent.

To obtain the highest strength, the optimal value of Na_2O/b ratio in BFS-AAM and FA-AAM is 5.5%-8% [178,180,181,184-186] and 7%-10% [187-191], respectively, while the optimal value of Na_2O/b ratio in BFS/FA-AAM is probably around 6–8% [10,183,192-195]. It is important to emphasize that BFS/FA-AAM with a high Na_2O/b ratio tends to have shrinkage cracks and leaching problems at an early age. Sealed curing has proved to be an effective condition for BFS/FA-AAM [10,196-198].

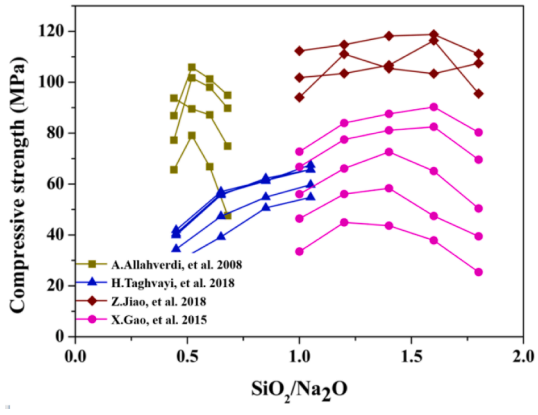

Fig. 15. Effect of SiO_2/Na_2O ratio on the compressive strength of BFS/FA-AAM [146,178,180,181].

4.3. SiO_2/Na_2O ratio

The effect of the SiO_2/Na_2O ratio on the compressive strength BFS/FA-AAM is shown in Fig. 15. The data includes both mortar and concrete samples. The highest compressive strength of BFS/FA-AAM could be obtained when the SiO_2/Na_2O ratio is at an optimal value [146,178,180,181,200]. With a higher SiO_2/Na_2O ratio, the dissolved network modifiers and intermediates could be absorbed by soluble Si more quickly. Gradually, a denser microstructure could be generated because more reaction products are formed in the solution [200]. Besides, reaction products with more Si-O-Si bonds are formed, leading to a higher degree of polymerization and higher strength.

However, when the SiO_2/Na_2O exceeds a particular value (around 0.6–1.5) [10,178,180,181,201], the strength begins to decrease. A Si layer may form on the surface of the BFS particles earlier with excess SiO_2/Na_2O, hindering the further dissolution of reaction ions. Less dissolution of reaction ions eventually prevents the formation of CASH gel, leading to a coarser microstructure [202]. On the other hand, excess SiO_2 species could form polymerized SiO_4 that consequently precipitate, which may suppress the precipitation of zeolite crystals and hinder the polymerization of NASH gel in the subsequent process.

Although many researchers have proved the existence of an optimal value [10,172]. The optimal value of SiO_2/Na_2O ratio in BFS-AAM and FA-AAM and BFS/FA-AAM is not always constant. The influence of the SiO_2/Na_2O ratio should be considered together with the Na_2O/b ratio and BFS/b. The highest strength can be reached only when the erosion rate of OH^- and the absorption rate of soluble Si reach a specific balance, and when the amount of supplied soluble Si and the amount of existing Si reaches a specific proportion.

4.4. w/b ratio

The effect of water on the strength of BFS/FA-AAM is not so large as that of OPC. One significant difference between them is that the formation of reaction products in BFS/FA-AAM requires nearly no water [135,203-205]. The reaction mechanism of BFS-AAM shows that water merely acts as an alkalis carrier while hardly reacting in the creation of CASH. In FA-AAM, water is consumed in the dissolution stage while released again in the polymerization process. Davidovits reported that water is not chemically bound to the structure of the matrix [204]. Although water is not the most decisive factor compared with the influence of the factors discussed above on the strength of BFS/FA-AAM, it still cannot be ignored. From the physical point of view, less water could lead to higher density and a slightly higher compressive strength. Besides, water content is an important factor concerning the workability of BFS/FA-AAM [10,206,207]. The water demand of AAM is affected by several factors, including particle size and shape distribution, and specific surface area [208].

The majority of researchers studied the relationships between the l/b ratio (the mass ratio of alkali-activated solution to binder) and the compressive strength and flowability, as shown in Fig. 16. The data includes both paste and concrete samples without using a superplasticizer. It is reasonable for the flowability to increase as the l/b ratio increases. However, it seems that l/b has little effect on the strength development of BFS/FA-AAM [9,167,171,209]. That is because the change of the l/b ratio is not only changing the w/b ratio (the mass ratio of water to binder) but also the Na_2O/b ratio. It is important to remark that the Na_2O/b ratio and w/b ratio may have the opposite effect on the strength. For example, for the alkali solution with high Na_2O content,

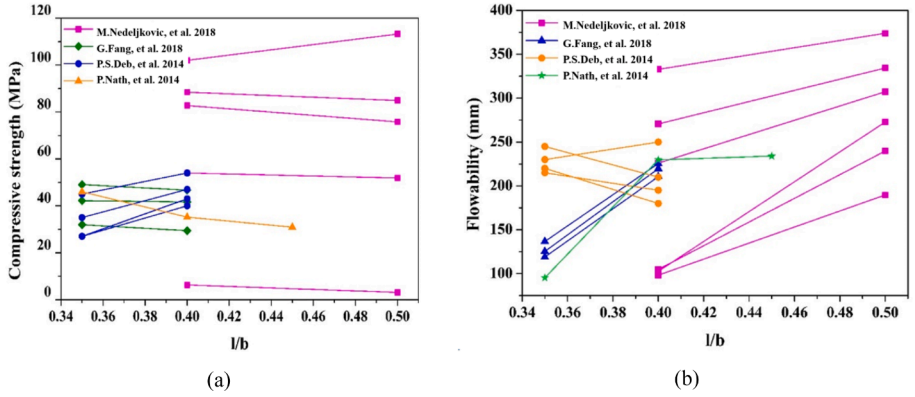

Fig. 16. Effect of l/b ratio on BFS/FA-AAM: (a) effect on compressive strength; (b) effect on flowablity [9,167,171,209].

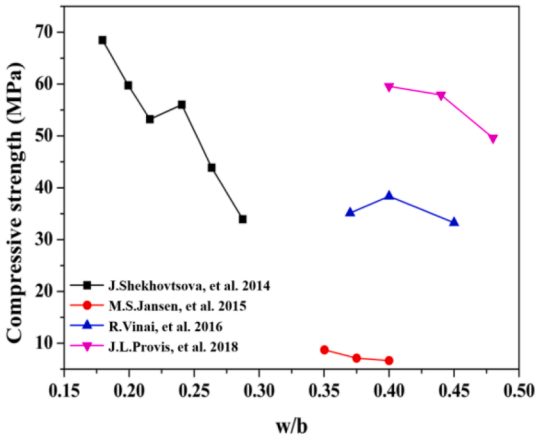

Fig. 17. Effect of w/b ratio on the compressive strength of BFS/FA-AAM [210-212,214].

increasing the l/b ratio may improve the strength. While for alkali solution with low Na_2O content, increasing the l/b ratio may greatly reduce the strength. Therefore, using the parameter l/b ratio in the mix design may lead to incomparable and unpredictable results between different researches. It is recommended to use the w/b ratio instead of the l/b ratio to obtain more precise results for further study.

Generally, the increase of the w/b ratio could reduce the compressive strength of BFS/FA-AAM [10,27,210], as shown in Fig. 17. J.L. Provis et al. [210] studied the effect of the w/b ratio on the strength of BFS-AAM. The results show that increasing the w/b ratio from 0.40 to 0.48 reduced the compressive strength by 10 MPa. J. Shekhovtsova et al. [211] investigate the effect of the w/b ratio on strength of the FA-alkali activated pastes. The results show that an increase in w/b from 0.18 to 0.29 could lead to a decrease in the compressive strength from 49 MPa to 21 MPa. M.S. Jansen et al. [212] reported that the strength of BFS-AAM primarily depends on the mix composition even though the w/b ratio did affect the strength of the mortar to some degree. R.Vinai et al. [213] indicated that the w/b ratio does not affect significantly the strength development except for high values (≥0.4).

5. Conclusions

A systematic review was conducted about BFS-AAM, FA-AAM and BFS/FA-AAM. Due to the different quality of raw materials, the strength may vary considerably. A selection of suitable precursors could be carried out based on the requirements that are summarized in this paper. Through the study of the reaction mechanism and reaction products of BFS-AAM, FA-AAM, and BFS/FA-AAM, a comprehensive understanding of the strength development could be obtained. The elaboration of the effect of different reaction ions on the reaction process provides a theoretical basis for the selection of control factors for strength development. Moreover, the demonstration of the effect of control factors on the strength and reaction process could provide some guidance for the mix design of BFS/FA-AAM. It is worth noting that a large amount of currently performed research on BFS/FA-AAM is focused on the general $NaOH/Na_2SiO_3$ ratio, alkaline activators/precursors ratio, and l/b ratio. Further studies of the properties of BFS/FA-AAM based on control factors are recommended to obtain more precise and comparable results.

Declaration of Competing Interest

The authors declare that they have no known competing financial interests or personal relationships that could have appeared to influence the work reported in this paper.

Acknowledgements

The first author would also like to gratefully acknowledge the China Scholarship Council (Grant Number 201806370216).

References

[1] F. Preston, J. Lehne, Making Concrete Change Innovation in Low-carbon Cement and Concrete, (2018).
[2] G. Habert, J.B.D.E. De Lacaillerie, N. Roussel, An environmental evaluation of geopolymer based concrete production: reviewing current research trends, J. Clean. Prod. 19 (11) (2011) 1229–1238.
[3] L.K. Turner, F.G. Collins, b. materials, Carbon dioxide equivalent (CO2-e) emissions: A comparison between geopolymer and OPC cement concrete, Constr. Build. Mater., 43 (2013) 125-130.
[4] J.S.J. van Deventer, J.L. Provis, P. Duxson, D.G. Brice, Chemical research and climate change as drivers in the commercial adoption of alkali activated materials, Waste Biomass Valorization 1 (1) (2010) 145–155.
[5] R.J. Thomas, H. Ye, A. Radlinska, S. Peethamparan, Alkali-activated slag cement concrete, J. Am. Concr. Inst. 38 (1) (2016) 33–38.
[6] S. Fang, E.S.S. Lam, B. Li, B. Wu, Effect of alkali contents, moduli and curing time on engineering properties of alkali activated slag, Constr. Build. Mater. 249 (2020), 118799.
[7] J.J. Chang, A study on the setting characteristics of sodium silicate-activated slag pastes, Cem. and Concr. Res. 33 (7) (2003) 1005–1011.
[8] C. Duran Atiş, C. Bilim, Özlem Çelik, O. Karahan, Influence of activator on the strength and drying shrinkage of alkali-activated slag mortar, Constr. Build. Mater. 23 (1) (2009) 548–555.
[9] M. Nedeljkovic, Z. Li, G. Ye, Setting, Strength, and Autogenous Shrinkage of Alkali-Activated Fly Ash and Slag Pastes: Effect of Slag Content, Materials 11 (11) (2018).
[10] B. Sun, Y. Sun, G. Ye, G. De Schutter, A mix design methodology of slag and fly ash-based alkali-activated paste, Cem. Concr. Compos. 126 (2022) 104368, https://doi.org/10.1016/j.cemconcomp.2021.104368.
[11] K. Arbi, M. Nedeljkovic, Y. Zuo, S. Grünewald, A. Keulen, G. Ye, Experimental study on workability of alkali activated fly ash and slag-based geopolymer concretes, An ECI conference (2015) 75–78.
[12] M. Nedeljkovic, K. Arbi, Y. Zuo, G. Ye, in: Physical properties and pore solution analysis of alkali activated fly ash-slag pastes, Lyngby, Denmark, 2016, pp. 22–24.

[13] M. Nedeljković, Y. Zuo, K. Arbi, G. Ye, Carbonation resistance of alkali-activated slag under natural and accelerated conditions, J. Sustain. Metall. 4 (1) (2018) 33–49.
[14] M. Nedeljković, Y. Zuo, K. Arbi, G. Ye, in: High Tech Concrete: Where Technology and Engineering Meet, Springer International Publishing, Cham, 2018, pp. 2213–2223, https://doi.org/10.1007/978-3-319-59471-2_253.
[15] Z. Tan, G. De Schutter, G. Ye, Y. Gao, Influence of particle size on the early hydration of slag particle activated by Ca (OH) 2 solution, Constr. Build. Mater. 52 (2014) 488–493.
[16] Y. Ma, J. Hu, G. Ye, The effect of activating solution on the mechanical strength, reaction rate, mineralogy, and microstructure of alkali-activated fly ash, J. Mater. Sci. 47 (11) (2012) 4568–4578.
[17] A.M. Fernandez-Jimenez, A. Palomo, C. Lopez-Hombrados, Engineering properties of alkali-activated fly ash concrete, ACI Mater. J. 103 (2) (2006) 106.
[18] M. Sofi, J.S.J. van Deventer, P.A. Mendis, G.C. Lukey, Engineering properties of inorganic polymer concretes (IPCs), Cem. Concr. Res. 37 (2) (2007) 251–257.
[19] A.M. Rashad, A comprehensive overview about the influence of different additives on the properties of alkali-activated slag–A guide for Civil Engineer, Constr. Build. Mater. 47 (2013) 29–55.
[20] M.O. Yusuf, M.A.M. Johari, Z.A. Ahmad, M. Maslehuddin, Design, Evolution of alkaline activated ground blast furnace slag–ultrafine palm oil fuel ash based concrete, Mater. Des. 55 (2014) 387–393.
[21] M.O. Yusuf, M.A.M. Johari, Z.A. Ahmad, M. Maslehuddin, Effects of H2O/Na2O molar ratio on the strength of alkaline activated ground blast furnace slag-ultrafine palm oil fuel ash based concrete, Mater. Des. 56 (2014) 158–164.
[22] R. Anuradha, V. Sreevidya, R. Venkatasubramani, B.V. Rangan, Modified guidelines for geopolymer concrete mix design using Indian standard, Asian, J. Civ. Eng. 13 (2012) 357–368.
[23] N. Li, C. Shi, Z. Zhang, H. Wang, Y. Liu, A review on mixture design methods for geopolymer concrete, Compos. B. Eng. 178 (2019), 107490.
[24] C. Li, H. Sun, L. Li, A review: The comparison between alkali-activated slag (Si+ Ca) and metakaolin (Si+ Al) cements, Cem. Concr. Res. 40 (9) (2010) 1341–1349.
[25] P. Duxson, J.L. Provis, Designing Precursors for Geopolymer Cements, J. Am. Ceram. Soc. 91 (12) (2008) 3864–3869.
[26] C. Shi, D. Roy, P. Krivenko, Alkali-activated cements and concretes, CRC press2003.
[27] S.-D. Wang, K.L. Scrivener, P.L. Pratt, Factors affecting the strength of alkali-activated slag, Cem. Concr. Res. 24 (6) (1994) 1033–1043.
[28] B. Talling, J. Brandstetr, Present state and future of alkali-activated slag concretes, J. Am. Concr. Inst. 114 (1989) 1519–1546.
[29] E. Douglas, J. Brandstetr, A preliminary study on the alkali activation of ground granulated blast-furnace slag, Cem. Concr. Res. 20 (5) (1990) 746–756.
[30] M.B. Haha, B. Lothenbach, G. Le Saout, F. Winnefeld, Influence of slag chemistry on the hydration of alkali-activated blast-furnace slag — Part I: Effect of MgO, Cem. Concr. Res. 41 (9) (2011) 955–963.
[31] M.B. Haha, B. Lothenbach, G. Le Saout, F. Winnefeld, Influence of slag chemistry on the hydration of alkali-activated blast-furnace slag — Part II: Effect of Al2O3, Cem. Concr. Res. 42 (1) (2012) 74–83.
[32] Y.S. Shkolnick, Physicochemical principles of the hydraulic activity of blast furnace slag, 8th international congress on the chemistry of cement, in: 8th international congress on the chemistry of cement, 1986, pp. 133–136.
[33] W.H. Zachariasen, The atomic arrangement in glass, J. Am. Ceram. Soc. 54 (10) (1932) 3841–3851.
[34] X. Chen, N. Yang, Influence of polymeric structure of granulated blast furnace slag on their hydraulic activities, 2nd Beijing International Symposium on Cement and Concrete, Beijing (1989) 346–351.
[35] N. Nakamura, M. Sakai, K. Koibuchi, Y. Iijima, Properties of High-Strength Concrete Incorporating Very Finely Ground Granulated Blast Furnace Slag, J. Am. Concr. Inst. 91 (1986) 1361–1380.
[36] P.Z. Wang, R. Trettin, V. Rudert, Effect of fineness and particle size distribution of granulated blast-furnace slag on the hydraulic reactivity in cement systems, Adv. Cem. Res. 17 (4) (2005) 161–167.
[37] H. Wan, Z. Shui, Z. Lin, Analysis of geometric characteristics of GGBS particles and their influences on cement properties, Cem. Concr. Res. 34 (1) (2004) 133–137.
[38] S. Caijun, L. Yinyu, Investigation on some factors affecting the characteristics of alkali-phosphorus slag cement, Cem. Concr. Res. 19 (4) (1989) 527–533.
[39] O.E. Gjorv, Alkali Activation of a Norwegian Granulated Blast-Furnace Slag, J. Am. Concr. Inst. 114 (1989) 1501–1518.
[40] ASTM C 1073, Test Method for Hydraulic Activity of Ground Slag by reaction with Alkali, Annual Book of ASTM Standards, Concrete and Aggregate, American Society for Testing &Materials (ASTM), Philadelphia, USA, 2003.
[41] P.K. Mehta, Concrete. Structure, properties and materials (1986).
[42] EN, 450–1, Fly ash for concrete, Definition, specifications and conformity criteria (2012).
[43] A. Fernández-Jiménez, A. Palomo, Composition and microstructure of alkali activated fly ash binder: Effect of the activator, Cem. Concr. Res. 35 (10) (2005) 1984–1992.
[44] S. Kumar, R. Kumar, T.C. Alex, A. Bandopadhyay, S.P. Mehrotra, Influence of reactivity of fly ash on geopolymerisation, Adv. Appl. Ceram. 106 (3) (2007) 120–127.
[45] R.J. Myers, B. Lothenbach, S.A. Bernal, J.L. Provis, Thermodynamic modelling of alkali-activated slag cements, Appl. Geochemistry 61 (2015) 233–247.
[46] A.M. Fernández Jiménez, Cementos de escorias activadas alcalinamente: influencia de las variables y modelización del proceso, (2000).
[47] A. Fernández-Jiménez, A. Palomo, Characterisation of fly ashes. Potential reactivity as alkaline cements☆, Fuel 82 (18) (2003) 2259–2265.
[48] RD Hooton, C. Shi, RL Day, Selectivity of alkaline activators for the activation of slags, Cem. Concrt. Agg. 18 (1) (1996) 8, https://doi.org/10.1520/CCA10306J.
[49] J.L. Provis, Activating solution chemistry for geopolymers, Geopolymers (2009) 50–71.
[50] E.I. Diaz-Loya, E.N. Allouche, S. Vaidya, Mechanical Properties of Fly-Ash-Based Geopolymer Concrete, ACI Mater. J. 108 (3) (2011) 300–306.
[51] M. Palacios, M.M. Alonso, C. Varga, F. Puertas, Influence of the alkaline solution and temperature on the rheology and reactivity of alkali-activated fly ash pastes, Cem. Concr. Compos. 95 (2019) 277–284.
[52] X.Y. Zhuang, L. Chen, S. Komarneni, C.H. Zhou, D.S. Tong, H.M. Yang, W.H. Yu, H. Wang, Fly ash-based geopolymer: clean production, properties and applications, J. Clean. Prod. 125 (2016) 253–267.
[53] A. Gharzouni, L. Ouamara, I. Sobrados, S. Rossignol, Alkali-activated materials from different aluminosilicate sources: Effect of aluminum and calcium availability, J. Non-Cryst. Solids 484 (2018) 14–25.
[54] P. Duxson, A. Fernández-Jiménez, J.L. Provis, G.C. Lukey, A. Palomo, J.S.J. van Deventer, Geopolymer technology: the current state of the art, J. Mater. Sci. 42 (9) (2007) 2917–2933.
[55] A. Fernández-Jiménez, A. Palomo, I. Sobrados, J. Sanz, The role played by the reactive alumina content in the alkaline activation of fly ashes, Microporous and Mesoporous Materials, Microporous Mesoporous Mater. 91 (1-3) (2006) 111–119.
[56] L. Weng, K. Sagoe-Crentsil, T. Brown, S. Song, Effects of aluminates on the formation of geopolymers, Mater. Sci. Eng. B 117 (2) (2005) 163–168.
[57] L.M. Keyte, Fly ash glass chemistry and inorganic polymer cements, Geopolymers (2009) 15–36.
[58] R.T. Chancey, P. Stutzman, M.C.G. Juenger, D.W. Fowler, Comprehensive phase characterization of crystalline and amorphous phases of a Class F fly ash, Cem. Concr. Res. 40 (1) (2010) 146–156.
[59] N.W. Chen-Tan, A. Van Riessen, C.V. Southam, Determining the reactivity of a fly ash for production of geopolymer, J. Am. Ceram. Soc., 92(4) (2009) 881-887.
[60] Z. Zhang, H. Wang, J.L. Provis, Quantitative study of the reactivity of fly ash in geopolymerization by FTIR, J. Sustain. Cem.-Based Mater. 1 (4) (2012) 154–166.
[61] I. Garcia-Lodeiro, A. Palomo, A. Fernández-Jiménez, in: Handbook of Alkali-Activated Cements, Mortars and Concretes, Elsevier, 2015, pp. 49–73, https://doi.org/10.1533/9781782422884.1.49.
[62] E.I. Diaz-Loya, E.N. Allouche, S.J.A.m.j. Vaidya, Mechanical properties of fly-ash-based geopolymer concrete 108 (3) (2011) 300.
[63] W.D.A. Rickard, R. Williams, J. Temuujin, A. van Riessen, Assessing the suitability of three Australian fly ashes as an aluminosilicate source for geopolymers in high temperature applications, Mater. Sci. Eng. 528 (9) (2011) 3390–3397.
[64] J.G.S. van Jaarsveld, J.S.J. van Deventer, G.C. Lukey, The characterisation of source materials in fly ash-based geopolymers, Mater. Lett. 57 (7) (2003) 1272–1280.
[65] S. Kumar, R. Kumar, Mechanical activation of fly ash: Effect on reaction, structure and properties of resulting geopolymer, Ceram. Int. 37 (2) (2011) 533–541.
[66] ASTM C 618, Standard Specification for Coal Fly Ash and Raw or Calcined Natural Pozzolan for Use in Concrete, Annual Book of ASTM Standards, American Society for Testing &Materials (ASTM), Philadelphia, USA, 2003.
[67] Sindhunata, J.S.J. van Deventer, G.C. Lukey, H. Xu, Xu, Effect of curing temperature and silicate concentration on fly-ash-based geopolymerization, Ind. Eng. Chem. Res. 45 (10) (2006) 3559–3568.
[68] E.G. Rochow, Soluble Silicates: Their Properties and Uses, J. Am. Chem. Soc. (1953).
[69] C.G. Knight, R. Balec, S. Kinrade, The structure of silicate anions in aqueous alkaline solutions, Angew. Chem. Int. 119 (43) (2007) 8296–8300.
[70] J.L. Provis, P. Duxson, G.C. Lukey, F. Separovic, W.M. Kriven, J.S.J. van Deventer, Modeling speciation in highly concentrated alkaline silicate solutions, Ind. Eng. Chem. Res. 44 (23) (2005) 8899–8908.
[71] X. Yang, W. Zhu, Q. Yang, The viscosity properties of sodium silicate solutions, J. Solut. Chem. 37 (1) (2008) 73–83.
[72] D. Krizan, B. Zivanovic, Effects of dosage and modulus of water glass on early hydration of alkali–slag cements, Cem. Concr. Res. 32 (8) (2002) 1181–1188.
[73] A.M.M. Al Bakri, H. Kamarudin, A.K. Omar, M.N. Norazian, C.M. Ruzaidi, The Effect Of Alkaline Activator Ratio On The Compressive Strength Of Fly Ash-Based geopolymers, Aust. J. Basic & Appl. Sci (2011).
[74] V. Glukhovsky, Ancient, modern and future concretes, First International Conference on Alkaline Cements and Concretes, Kiev, Ukraine, (1994) 1-9.
[75] B. Lothenbach, A. Gruskovnjak, Hydration of alkali-activated slag: thermodynamic modelling, Adv. Cem. Res. 19 (2) (2007) 81–92.
[76] E. Altan, S.T. Erdoğan, Alkali activation of a slag at ambient and elevated temperatures, Cem. Concr. Compos. 34 (2) (2012) 131–139.
[77] D. Ravikumar, N. Neithalath, Effects of activator characteristics on the reaction product formation in slag binders activated using alkali silicate powder and NaOH, Cem. Concr. Compos. 34 (7) (2012) 809–818.
[78] B.S. Gebregziabiher, R. Thomas, S. Peethamparan, Very early-age reaction kinetics and microstructural development in alkali-activated slag, Cem. Concr. Compos. 55 (2015) 91–102.
[79] D. Ravikumar, N. Neithalath, Reaction kinetics in sodium silicate powder and liquid activated slag binders evaluated using isothermal calorimetry, Thermochim. Acta 546 (2012) 32–43.
[80] E. Deir, B.S. Gebregziabiher, S. Peethamparan, Influence of starting material on the early age hydration kinetics, microstructure and composition of binding gel in alkali activated binder systems, Cem. Concr. Compos. 48 (2014) 108–117.

[81] Z. Sun, A. Vollpracht, Isothermal calorimetry and in-situ XRD study of the NaOH activated fly ash, metakaolin and slag, Cem. Concr. Res. 103 (2018) 110–122.
[82] Y. Zuo, Experimental Study and Numerical Simulation of the Reaction Process and Microstructure Formation of Alkali-Activated Materials, Delft University of Technology, 2019.
[83] A. Kashani, J.L. Provis, G.G. Qiao, J.S.J. van Deventer, The interrelationship between surface chemistry and rheology in alkali activated slag paste, Constr. Build. Mater., 65 (2014) 583-591.
[84] Z. Huanhai, W. Xuequan, X. Zhongzi, T. Mingshu, Kinetic study on hydration of alkali-activated slag, Cem. Concr. Res. 23 (6) (1993) 1253–1258.
[85] N. Li, C. Shi, Z. Zhang, Understanding the roles of activators towards setting and hardening control of alkali-activated slag cement, Compos. B. Eng. 171 (2019) 34–45.
[86] A.R. Sakulich, D.P. Bentz, Mitigation of autogenous shrinkage in alkali activated slag mortars by internal curing, Mater. Struct. 46 (8) (2013) 1355–1367.
[87] M. Palacios, F. Puertas, Effect of shrinkage-reducing admixtures on the properties of alkali-activated slag mortars and pastes, Cem. Concr. Res. 37 (5) (2007) 691–702.
[88] A.R. Brough, M. Holloway, J. Sykes, A. Atkinson, Sodium silicate-based alkali-activated slag mortars: Part II. The retarding effect of additions of sodium chloride or malic acid, Cem. Concr. Res. 30 (9) (2000) 1375–1379.
[89] T. Luukkonen, H. Sreenivasan, Z. Abdollahnejad, J. Yliniemi, A. Kantola, V. V. Telkki, P. Kinnunen, M. Illikainen, Influence of sodium silicate powder silica modulus for mechanical and chemical properties of dry-mix alkali-activated slag mortar, Constr. Build. Mater. 233 (2020), 117354.
[90] K. Vance, M. Aguayo, A. Dakhane, D. Ravikumar, J. Jain, N. Neithalath, Microstructural, mechanical, and durability related similarities in concretes based on OPC and alkali-activated slag binders, Int. J. Concr. Struct. Mater 8 (4) (2014) 289–299.
[91] D.B. Kumarappa, S. Peethamparan, M. Ngami, Autogenous shrinkage of alkali activated slag mortars: Basic mechanisms and mitigation methods, Cem. Concr. Res. 109 (2018) 1–9.
[92] S. Liu, Q. Li, W. Han, Effect of various alkalis on hydration properties of alkali-activated slag cements, J. Therm. Anal. Calorim. 131 (3) (2018) 3093–3104.
[93] M. Almakhadmeh, A. Soliman, B. Materials, Effects of mixing water temperatures on properties of one-part alkali-activated slag paste, Constr. Build. Mater. 266 (2021), 121030.
[94] Z. Li, M. Wyrzykowski, H. Dong, J. Granja, M. Azenha, P. Lura, G. Ye, Internal curing by superabsorbent polymers in alkali-activated slag, Cem. Concr. Res. 135 (2020), 106123.
[95] A. Hajimohammadi, T. Ngo, P. Mendis, A. Kashani, J.S.J. van Deventer, Alkali activated slag foams: the effect of the alkali reaction on foam characteristics, J. Clean. Prod. 147 (2017) 330–339.
[96] S. Choi, K.M. Lee, Influence of Na2O content and Ms (SiO2/Na2O) of alkaline activator on workability and setting of alkali-activated slag paste, Mater. 12 (13) (2019) 2072.
[97] C. Shi, R.L. Day, A calorimetric study of early hydration of alkali-slag cements, Cem. Concr. Res. 25 (6) (1995) 1333–1346.
[98] K.L. Scrivener, A. Bentur, P.L. Pratt, Quantitative characterization of the transition zone in high strength concretes, Adv. Cem. Res. 1 (4) (1988) 230–237.
[99] S.-D. Wang, K.L. Scrivener, Hydration products of alkali activated slag cement, Cem. Concr. Res. 25 (3) (1995) 561–571.
[100] I.G. Richardson, The calcium silicate hydrates, Cem. Concr. Res. 38 (2008) 137–158.
[101] F. Puertas, A. Fernández-Jiménez, M.T. Blanco-Varela, Pore solution in alkali-activated slag cement pastes. Relation to the composition and structure of calcium silicate hydrate, Cem. Concr. Res. 34 (2004) 139–148.
[102] J.I. Escalante-García, A.F. Fuentes, A. Gorokhovsky, P.E. Fraire-Luna, G. J. Mendoza-Suarez, Hydration products and reactivity of blast-furnace slag activated by various alkalis, J. Am. Ceram. Soc. 86 (2003) 2148–2153.
[103] I. Ismail, S.A. Bernal, J.L. Provis, R. San Nicolas, D.G. Brice, A.R. Kilcullen, S. Hamdan, J.S.J, van Deventer, Influence of fly ash on the water and chloride permeability of alkali-activated slag mortars and concretes, Constr. Build. Mater. 48 (2013) 1187–1201.
[104] J.L. LaRosa, S. Kwan, M.W. Grutzeck, Zeolite formation in class F fly ash blended cement pastes, J. Am. Ceram. Soc. 75 (1992) 1574–1580.
[105] Q. Cheng, A. Tagnit-Hamou, S.L. Sarkar, Strength and microstructural properties of water glass activated slag, MRS Online Proceedings 245 (1991) 49–54.
[106] A. Roy, P.J. Schilling, H.C. Eaton, P.G. Malone, W.N. Brabston, L.D. Wakeley, Activation of ground blast-furnace slag by alkali-metal and alkaline-Earth hydroxides, J. Am. Ceram. Soc. 75 (1992) 3233–3240.
[107] S.D. Wang, X.C. Pu, K.L. Scrivener, P.L. Pratt, Alkali-activated slag cement and concrete: a review of properties and problems, Adv. Cem. Res. 7 (1995) 93–102.
[108] F. Puertas, Cementos de escorias activadas alcalinamente: Situación actual y perspectivas de futuro, 1995.
[109] A. Fernández-Jiménez, F. Puertas, L. Fernández-Carrasco, Procesos de activación alcalino-sulfáticos de una escoria española de alto horno, 2006.
[110] A. Palomo, M.W. Grutzeck, M.T. Blanco, Alkali-activated fly ashes: A cement for the future, Cem. Concr. Res. 29 (1999) 1323–1329.
[111] P. Duxson, S.W. Mallicoat, G.C. Lukey, W.M. Kriven, J.S.J. van Deventer, The effect of alkali and Si/Al ratio on the development of mechanical properties of metakaolin-based geopolymers, Colloids Surf. A: Physicochem. Eng. Asp. 292 (1) (2007) 8–20.
[112] C.K. Yip, G.C. Lukey, J.S.J. van Deventer, The coexistence of geopolymeric gel and calcium silicate hydrate at the early stage of alkaline activation, Cem. Concr. Res. 35 (2005) 1688–1697.
[113] Á. Palomo, E. Kavalerova, A. Fernández-Jiménez, P. Krivenko, I. García-Lodeiro, O. Maltseva, A review on alkaline activation: new analytical perspectives, 2015.
[114] A. Fernández-Jiménez, F. Puertas, I. Sobrados, J. Sanz, Structure of calcium silicate hydrates formed in alkaline-activated slag: influence of the type of alkaline activator, J. Am. Ceram. Soc. 86 (2003) 1389–1394.
[115] J.L. Provis, P. Duxson, J.S.J. Van Deventer, G.C. Lukey, The role of mathematical modelling and gel chemistry in advancing geopolymer technology, Chem. Eng. Res. Des. 83 (2005) 853–860.
[116] M.B. Haha, G. Le Saout, F. Winnefeld, B. Lothenbach, Influence of activator type on hydration kinetics, hydrate assemblage and microstructural development of alkali activated blast-furnace slags, Cem. Concr. Res. 41 (2011) 301–310.
[117] J.G.S. van Jaarsveld, J.S.J. Van Deventer, Effect of the alkali metal activator on the properties of fly ash-based geopolymers, Ind. Eng. Chem. Res. 38 (1999) 3932–3941.
[118] I.G. Richardson, A.R. Brough, G.W. Groves, C.M. Dobson, The characterization of hardened alkali-activated blast-furnace slag pastes and the nature of the calcium silicate hydrate (CSH) phase, Cem. Concr. Res. 24 (1994) 813–829.
[119] A.R. Brough, A. Atkinson, Sodium silicate-based, alkali-activated slag mortars: Part I. Strength, hydration and microstructure, Cem. Concr. Res. 32 (2002) 865–879.
[120] Z. Liu, D. Zhang, L. Li, J. Wang, N. Shao, D. Wang, Microstructure and phase evolution of alkali-activated steel slag during early age, Constr. Build. Mater. 204 (2019) 158–165.
[121] J.L. Provis, J.S.J. Van Deventer, Geopolymerisation kinetics. 1. In situ energy-dispersive X-ray diffractometry, Chem. Eng. Sci. 62 (2007) 2309–2317.
[122] J.L. Provis, J.J.C., Van Deventer, Geopolymerisation kinetics. 2. Reaction kinetic modelling, Chem. Eng. Sci. 62 (2007) 2318–2329.
[123] C. Li, Y. Li, H. Sun, L. Li, The composition of fly ash glass phase and its dissolution properties applying to geopolymeric materials, J. Am. Ceram. Soc. 94 (2011) 1773–1778.
[124] C. Chen, W. Gong, W. Lutze, I.L. Pegg, J. Zhai, Kinetics of fly ash leaching in strongly alkaline solutions, J. Mater. Sci. 46 (2011) 590–597.
[125] J.G. Jang, N.K. Lee, H.K. Lee, Fresh and hardened properties of alkali-activated fly ash/slag pastes with superplasticizers, Constr. Build. Mater. 50 (2014) 169–176.
[126] S.K. Nath, S. Kumar, Reaction kinetics, microstructure and strength behavior of alkali activated silico-manganese (SiMn) slag – Fly ash blends, Constr. Build. Mater. 147 (2017) 371–379.
[127] J.P. Hamilton, S.L. Brantley, C.G. Pantano, L.J. Criscenti, J. Kubicki, Dissolution of nepheline, jadeite and albite glasses: toward better models for aluminosilicate dissolution, Geochim. Cosmochim. 65 (2001) 3683–3702.
[128] G. Fang, Q. Wang, M. Zhang, In-situ X-ray tomographic imaging of microstructure evolution of fly ash and slag particles in alkali-activated fly ash-slag paste, Compos. B. Eng. 224 (2021), 109221.
[129] A.E. Blum, A.C. Lasaga, The role of surface speciation in the dissolution of albite, Geochim. Cosmochim. 55 (1991) 2193–2201.
[130] E.H. Oelkers, S.R. Gislason, The mechanism, rates and consequences of basaltic glass dissolution: I. An experimental study of the dissolution rates of basaltic glass as a function of aqueous Al, Si and oxalic acid concentration at 25 C and pH= 3 and 11, Geochim. Cosmochim. 65 (2001) 3671–3681.
[131] P. Duxson, G.C. Lukey, F. Separovic, J.S.J. Van Deventer, Effect of alkali cations on aluminum incorporation in geopolymeric gels, Ind. Eng. Chem. Res. 44 (2005) 832–839.
[132] R.K. Ilera, Allumina on the solubility of amorphous silica in water, J. Colloid Interface Sci. 43 (1973) 399–408.
[133] A. Fernández-Jiménez, A. Palomo, M. Criado, Microstructure development of alkali-activated fly ash cement: a descriptive model, Cem. Concr. Res. 35 (2005) 1204–1209.
[134] S. Chithiraputhiran, N. Neithalath, Isothermal reaction kinetics and temperature dependence of alkali activation of slag, fly ash and their blends, Constr. Build. Mater. 45 (2013) 233–242.
[135] F. Skvara, L. Kopecky, V. Smilauer, Z. Bittnar, Material and structural characterization of alkali activated low-calcium brown coal fly ash, J. Hazard. Mater. 168 (2009) 711–720.
[136] Y. Zuo, M. Nedeljković, G. Ye, Pore solution composition of alkali-activated slag/fly ash pastes, Cem. Concr. Res. 115 (2019) 230–250.
[137] S.K. Lee, J.F. Stebbins, Disorder and the extent of polymerization in calcium silicate and aluminosilicate glasses: O-17 NMR results and quantum chemical molecular orbital calculations, Geochim. Cosmochim. 70 (2006) 4275–4286.
[138] A. Rafeet, R. Vinai, M. Soutsos, W. Sha, Effects of slag substitution on physical and mechanical properties of fly ash-based alkali activated binders (AABs), Cem. Concr. Res. 122 (2019) 118–135.
[139] F. Winnefeld, A. Leemann, M. Lucuk, P. Svoboda, M. Neuroth, Assessment of phase formation in alkali activated low and high calcium fly ashes in building materials, Constr. Build. Mater. 24 (2010) 1086–1093.
[140] W. Tu, Y. Zhu, G. Fang, X. Wang, M. Zhang, Internal curing of alkali-activated fly ash-slag pastes using superabsorbent polymer, Cem. Concr. Res. 116 (2019) 179–190.
[141] C. Shi, A.F. Jiménez, A. Palomo, New cements for the 21st century: The pursuit of an alternative to Portland cement, Cem. Concr. Res. 41 (2011) 750–763.
[142] A. Palomo, S. Alonso, A. Fernandez-Jiménez, I. Sobrados, J. Sanz, Alkaline activation of fly ashes: NMR study of the reaction products, J. Am. Ceram. Soc., 87 (2004) 1141-1145.
[143] J. Davidovits, Geopolymer, green chemistry and sustainable development solutions: proceedings of the world congress geopolymer 2005, Geopolymer Institute2005.

[144] W. Loewenstein, P. Materials, The distribution of aluminum in the tetrahedra of silicates and aluminates, Am. Mineral., 39 (1954) 92-96.
[145] S. Kumar, R. Kumar, S.P. Mehrotra, Influence of granulated blast furnace slag on the reaction, structure and properties of fly ash based geopolymer, J. Mater. Sci. 45 (2010) 607–615.
[146] X. Gao, Q.L. Yu, H.J.H. Brouwers, Reaction kinetics, gel character and strength of ambient temperature cured alkali activated slag–fly ash blends, Constr. Build. Mater. 80 (2015) 105–115.
[147] B. Singh, M.R. Rahman, R. Paswan, S.K. Bhattacharyya, Effect of activator concentration on the strength, ITZ and drying shrinkage of fly ash/slag geopolymer concrete, Constr. Build. Mater. 118 (2016) 171–179.
[148] G. Fang, H. Bahrami, M. Zhang, Mechanisms of autogenous shrinkage of alkali-activated fly ash-slag pastes cured at ambient temperature within 24 h, Constr. Build. Mater. 171 (2018) 377–387.
[149] J.F. Stebbins, Z. Xu, NMR evidence for excess non-bridging oxygen in an aluminosilicate glass, Nature 390 (1997) 60–62.
[150] S. Puligilla, X. Chen, P. Mondal, Structures, Does synthesized CSH seed promote nucleation in alkali activated fly ash-slag geopolymer binder? Mater. Struct. 52 (2019) 1–13.
[151] I. Garcia-Lodeiro, A. Palomo, A. Fernández-Jiménez, D.E. Macphee, Compatibility studies between NASH and CASH gels. Study in the ternary diagram Na2O–CaO–Al2O3–SiO2–H2O, Cem. Concr. Res. 41 (2011) 923–931.
[152] I. Ismail, S.A. Bernal, J.L. Provis, R. San Nicolas, S. Hamdan, J.S.J., van Deventer, Modification of phase evolution in alkali-activated blast furnace slag by the incorporation of fly ash, Cem. Concr. Compos. 45 (2014) 125–135.
[153] S.-D. Wang, K.L. Scrivener, 29Si and 27Al NMR study of alkali-activated slag, Cem. Concr. Res. 33 (5) (2003) 769–774.
[154] G. Engelhardt, D. Michel, High-resolution solid-state NMR of silicates and zeolites, 1987.
[155] H. Xu, J.S.J. Van Deventer, Geopolymerisation of multiple minerals, Miner. Eng. 15 (2002) 1131–1139.
[156] J.W. Phair, J.S.J. Van Deventer, Effect of silicate activator pH on the leaching and material characteristics of waste-based inorganic polymers, Miner. Eng. 14 (2001) 289–304.
[157] W.K.W. Lee, J.S.J. van Deventer, Structural reorganisation of class F fly ash in alkaline silicate solutions, Colloids Surf. A: Physicochem. Eng. Asp. 211 (1) (2002) 49–66.
[158] M. Minaøíková, F.J.C.S. Škvára, Fixation of heavy metals in geopolymeric materials based on brown coal fly ash, Ceram. 50 (2006) 200–207.
[159] G. Sposito, The environmental chemistry of aluminum, CRC Press, 1995.
[160] E.N. Kani, A. Allahverdi, J.L. Provis, Efflorescence control in geopolymer binders based on natural pozzolan, Cem. Concr. Compos. 34 (2012) 25–33.
[161] F. Škvára, L. Kopecký, L. Myšková, V. Šmilauer, L. Alberovska, L.J. Vinšová, Aluminosilicate polymers–influence of elevated temperatures, efflorescence, Ceram. 53 (2009) 276–282.
[162] N.K. Lee, H.K. Lee, Reactivity and reaction products of alkali-activated, fly ash/slag paste, Constr. Build. Mater. 81 (2015) 303–312.
[163] M. Criado, A. Fernández Jiménez, I. Sobrados, A. Palomo, J. Sanz, Effect of relative humidity on the reaction products of alkali activated fly ash, J. Eur. Ceram. Soc. 32 (2012) 2799–2807.
[164] N.K. Lee, H.K. Lee, Setting and mechanical properties of alkali-activated fly ash/slag concrete manufactured at room temperature, Constr. Build. Mater. 47 (2013) 1201–1209.
[165] S. Saha, C. Rajasekaran, Enhancement of the properties of fly ash based geopolymer paste by incorporating ground granulated blast furnace slag, Constr. Build. Mater. 146 (2017) 615–620.
[166] A. Rafeet, R. Vinai, M. Soutsos, W. Sha, Guidelines for mix proportioning of fly ash/GGBS based alkali activated concretes, Constr. Build. Mater. 147 (2017) 130–142.
[167] P.S. Deb, P. Nath, P.K. Sarker, The effects of ground granulated blast-furnace slag blending with fly ash and activator content on the workability and strength properties of geopolymer concrete cured at ambient temperature, Mater. Des. 62 (2014) 32–39.
[168] P.S. Deb, P. Nath, P.K. Sarker, Drying Shrinkage of Slag Blended Fly Ash Geopolymer Concrete Cured at Room Temperature, Procedia Eng. 125 (2015) 594–600.
[169] K.K. Ramagiri, D.R. Chauhan, S. Gupta, A. Kar, D. Adak, A. Mukherjee, High-temperature performance of ambient-cured alkali-activated binder concrete, Innovative Infrastructure Solutions, Innov. Infrastruct. Solut. 6 (2) (2021), https://doi.org/10.1007/s41062-020-00448-y.
[170] G. Mounika, B. Ramesh, J.S. Kalyana Rama, Experimental investigation on physical and mechanical properties of alkali activated concrete using industrial and agro waste, Mater. Today Proc. 33 (2020) 4372–4376.
[171] P. Nath, P.K. Sarker, Effect of GGBFS on setting, workability and early strength properties of fly ash geopolymer concrete cured in ambient condition, Constr. Build. Mater. 66 (2014) 163–171.
[172] S. Zhang, Z. Li, B. Ghiassi, S. Yin, G. Ye, Fracture properties and microstructure formation of hardened alkali-activated slag/fly ash pastes, Cem. Concr. Res. 144 (2021), 106447.
[173] A. Mehta, R. Siddique, T. Ozbakkaloglu, F. Uddin Ahmed Shaikh, R. Belarbi, Fly ash and ground granulated blast furnace slag-based alkali-activated concrete: Mechanical, transport and microstructural properties, Constr. Build. Mater., 257 (2020).
[174] G. Fang, M. Zhang, Multiscale micromechanical analysis of alkali-activated fly ash-slag paste, Cem. Concr. Res. 135 (2020), 106141.
[175] K. Sankar, P. Stynoski, G.K. Al-Chaar, W.M. Kriven, Sodium silicate activated slag-fly ash binders: Part I-Processing, microstructure, and mechanical properties, J. Am. Ceram. Soc. 101 (6) (2018) 2228–2244.
[176] A. Kar, Characterizations of concretes with alkali-activated binder and correlating their properties from micro-to specimen level, 2013.
[177] R. Gopalakrishnan, K. Chinnaraju, Durability of ambient cured alumina silicate concrete based on slag/fly ash blends against sulfate environment, Constr. Build. Mater. 204 (2019) 70–83.
[178] A. Allahverdi, E.N. Kani, S. Esmaeilpoor, Engineering, Effects of silica modulus and alkali concentration on activation of blast-furnace slag, Iran. J. Mater. Sci. Eng. 5 (2008) 32–35.
[179] A. Allahverdi, B. Shaverdi, K.E. Najafi, Influence of Sodium Oxide on Properties of Fresh and harden paste of alkali activated blast furnace slag, Int. J. Civ. Eng. 8 (2010) 304–314.
[180] H. Taghvayi, K. Behfarnia, M. Khalili, The Effect of Alkali Concentration and Sodium Silicate Modulus on the Properties of Alkali-Activated Slag Concrete, J. Adv. Concr. Technol. 16 (2018) 293–305.
[181] Z. Jiao, Y. Wang, W. Zheng, W. Huang, Effect of Dosage of Alkaline Activator on the Properties of Alkali-Activated Slag Pastes, Adv. Mater. Sci. Eng. 2018 (2018) 1–12.
[182] Y. Ding, Experimental study on fracture properties of alkali-activated concrete, 2017.
[183] A.M. Humad, A. Kothari, J.L. Provis, A. Cwirzen, The Effect of Blast Furnace Slag/Fly Ash Ratio on Setting, Strength, and Shrinkage of Alkali-Activated Pastes and Concretes, Front. Mater. Sci. 6 (2019).
[184] K. Behfarnia, H. Taghvayi, M.B. Khalili Khasraghi, The Effect of Alkaline Activator on Workability and Compressive Strength of AlkaliActivated Slag Concrete, AUT j. civil eng. (2017).
[185] A.N. Hashim, K. Hussin, N. Begum, M.M. Al Bakri Abdullah, K. Abdul Razak, J. J. Ekaputri, Effect of Sodium Hydroxide (NaOH) Concentration on Compressive Strength of Alkali-Activated Slag (AAS) Mortars, Appl. Mech. Mater. 754-755 (2015) 300–304.
[186] N. Li, C. Shi, Z. Zhang, D. Zhu, H.-J. Hwang, Y. Zhu, T. Sun, A mixture proportioning method for the development of performance-based alkali-activated slag-based concrete, Cem. Concr. Compos. 93 (2018) 163–174.
[187] J.Š. František Škvára, Jan Bohunek and Alena Marková, Alkali-activatedb fly ash geopolymeric materials, (2003).
[188] M. Kaur, J. Singh, M. Kaur, Effect of alkali activator solution on the strength of fly ash based geopolymer mortar.
[189] F.A. Memon, M.F. Nuruddin, S. Khan, N. Shafiq, T. Ayub, Effect of sodium hydroxide concentration on fresh properties and compressive strength of self compacting geopolymer concrete, J. Eng. Sci. 8 (2013) 44–56.
[190] M.A. H. Bakkali, I. Frar, NaOH alkali-activated class F fly ash NaOH molarity, Curing conditions and mass ratio effect, (2016).
[191] J. Liyana, A.M.M. Al Bakri, K. Hussin, C.M. Ruzaidi, A.R. Azura, Effect of Fly Ash/Alkaline Activator Ratio and Sodium Silicate/NaOH Ratio on Fly Ash Geopolymer Coating Strength, Key Eng. Mater. 594–595 (2014) 146–150.
[192] A. Kothari, Effects of Fly Ash on the properties of Alkali Activated Slag, Concrete (2017).
[193] D. Bondar, S.V. Nanukuttan, M.N. Soutsos, P.M. Basheer, J.L. Provis, Suitability of alkali activated GGBS/Fly ash concrete for chloride environments, J. Am. Concr. Inst. 35 (2017) 31–35.
[194] Y. Ding, C. Shi, N. Li, Fracture properties of slag/fly ash-based geopolymer concrete cured in ambient temperature, Construction and Building Materials, Constr. Build. Mater. 190 (2018) 787–795.
[195] V. Athira, A. Bahurudeen, M. Saljas, K. Jayachandran, Influence of different curing methods on mechanical and durability properties of alkali activated binders, Constr. Build. Mater. 299 (2021), 123963.
[196] F. Collins, J.G. Sanjayan, Microcracking and strength development of alkali activated slag concrete, Cem. Concr. Compos. 23 (2001) 345–352.
[197] M. Nedeljković, B. Ghiassi, S. van der Laan, Z. Li, G. Ye, Effect of curing conditions on the pore solution and carbonation resistance of alkali-activated fly ash and slag pastes, Cem. Concr. Res. 116 (2019) 146–158.
[198] M. Hojati, A. Radlińska, Shrinkage and strength development of alkali-activated fly ash-slag binary cements, Constr. Build. Mater. 150 (2017) 808–816.
[199] A.M. Humad, A. Kothari, J.L. Provis, A. Cwirzen, The effect of blast furnace slag/fly ash ratio on setting, strength, and shrinkage of alkali-activated pastes and concretes, Front. Mater. Sci. 6 (2019) 9.
[200] X. Hu, C. Shi, Z. Shi, L. Zhang, Compressive strength, pore structure and chloride transport properties of alkali-activated slag/fly ash mortars, Cem. Concr. Compos. 104 (2019), 103392.
[201] A.V. Lăzărescu, H. Szilagyi, C. Baeră, A. Ioani, The Effect of Alkaline Activator Ratio on the Compressive Strength of Fly Ash-Based Geopolymer Paste, IOP Conf, Ser.: Mater. Sci. Eng. 209 (2017) 012064, https://doi.org/10.1088/1757-899X/209/1/012064.
[202] X. Ouyang, Y. Ma, Z. Liu, J. Liang, G. Ye, Effect of the sodium silicate modulus and slag content on fresh and hardened properties of alkali-activated fly ash/slag, Mater. 10 (2020) 15.
[203] H. Xu, J.S.J. van Deventer, The effect of alkali metals on the formation of geopolymeric gels from alkali-feldspars, Colloids Surf. A: Physicochem. Eng. Asp. 216 (1-3) (2003) 27–44.
[204] J. Davidovits, Geopolymer chemistry and properties, Geopolymer (1988) 25–48.
[205] D. Hardjito, B.V. Rangan, Development and properties of low-calcium fly ash-based geopolymer concrete, 2005.

[206] X. Dai, S. Aydin, M.Y. Yardimci, K. Lesage, G. De Schutter, Influence of water to binder ratio on the rheology and structural build-up of alkali-activated slag/fly ash mixtures, Constr. Build. Mater. 264 (2020), 120253.
[207] S.Y. Oderji, B. Chen, C. Shakya, M.R. Ahmad, S. Shah, Influence of superplasticizers and retarders on the workability and strength of one-part alkali-activated fly ash/slag binders cured at room temperature, Constr. Build. Mater. 229 (2019), 116891.
[208] P. Hewlett, M. Liska, Lea's chemistry of cement and concrete, Butterworth-Heinemann2019.
[209] G. Fang, W.K. Ho, W. Tu, M. Zhang, Workability and mechanical properties of alkali-activated fly ash-slag concrete cured at ambient temperature, Constr. Build. Mater. 172 (2018) 476–487.
[210] S.A. Bernal, J.L. Provis, J.S.J. van Deventer, Impact of water content on the performance of alkali-activated slag concretes, 2019.
[211] J. Shekhovtsova, E.P. Kearsley, M. Kovtun, Effect of activator dosage, water-to-binder-solids ratio, temperature and duration of elevated temperature curing on the compressive strength of alkali-activated fly ash cement pastes, J. S. Afr. Inst. Civ. Eng. 56 (2014) 44–52.
[212] M.S. Jansen, M.U. Christiansen, Effect of Water-solids ratio on the compressive strength and morphology of fly ash-waste glass geopolymer mortars, World of Coal Ash (WOCA) Conference, Nasvhille, TN, 2015.
[213] R. Vinai, A. Rafeet, M. Soutsos, W. Sha, The Role of Water Content and Paste Proportion on Physico-mechanical Properties of Alkali Activated Fly Ash-Ggbs Concrete, J. Sustain. Metall. 2 (1) (2016) 51–61.
[214] M. Soutsos, A.P. Boyle, R. Vinai, A. Hadjierakleous, S.J. Barnett, Factors influencing the compressive strength of fly ash based geopolymers, Constr. Build. Mater. 110 (2016) 355–368.